Cell Reports
Medicine

Article

The SGLT2 inhibitor dapagliflozin ameliorates renal fibrosis in hyperuricemic nephropathy

Graphical abstract

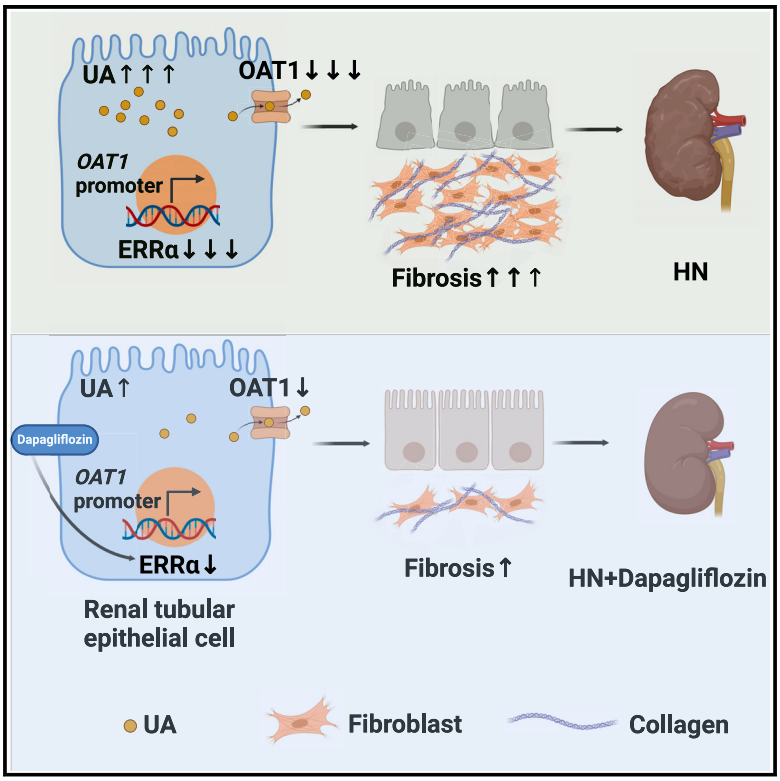

Highlights

- Dapagliflozin mitigates renal fibrosis and enhances renal function in HN
- Dapagliflozin activates ERRα to regulate UA transporters, enhancing UA excretion
- Dapagliflozin alleviates tubular injury and TIF by restoring mitochondrial function
- The ERRα-OAT1 axis is vital in HN pathogenesis and is a potential therapeutic target

Authors

Hongtu Hu, Weiwei Li, Yiqun Hao, ..., Ying Zhou, Wei Liang, Yun Cao

Correspondence

zhouying2018@whu.edu.cn (Y.Z.), dr.liangwei@whu.edu.cn (W.L.), yuncao1223@hainmc.edu.cn (Y.C.)

In brief

Hu et al. elucidate that the SGLT2 inhibitor dapagliflozin significantly attenuates renal fibrosis and dysfunction in hyperuricemic nephropathy by targeting ERRα. This study underscores the therapeutic potential of the ERRα-OAT1 axis in enhancing uric acid excretion and ameliorating kidney damage.

Hu et al., 2024, Cell Reports Medicine 5, 101690
August 20, 2024
https://doi.org/10.1016/j.xcrm.2024.101690

CellPress

Cell Reports Medicine

CellPress
OPEN ACCESS

Article

The SGLT2 inhibitor dapagliflozin ameliorates renal fibrosis in hyperuricemic nephropathy

Hongtu Hu,[2,6,7,9] Weiwei Li,[3,9] Yiqun Hao,[2] Zhuan Peng,[2] Zhengping Zou,[4,5] Jiali Wei,[1] Ying Zhou,[8,*] Wei Liang,[2,6,*] and Yun Cao[1,10,*]

[1]Department of Nephrology, Hainan General Hospital (Hainan Affiliated Hospital of Hainan Medical University), Haikou, China
[2]Division of Nephrology, Renmin Hospital of Wuhan University, Wuhan, China
[3]Division of Nephrology, The Central Hospital of Enshi Tujia and Miao Autonomous Prefecture, No. 158 Wuyang Avenue, Enshi, China
[4]Division of Nephrology, Qianjiang Hospital Affiliated to Renmin Hospital of Wuhan University, Wuhan, China
[5]Qianjiang Clinical Medical College, Health Science Center, Yangtze University, Jingzhou, China
[6]Key Clinical Research Center of Kidney Disease in Hubei, 238 Jiefang Road, Wuhan, China
[7]Central Laboratory, Renmin Hospital of Wuhan University, Wuhan, China
[8]Department of Radiology and Nuclear Medicine, Xuanwu Hospital, Capital Medical University, No. 45 Changchun St, Xicheng District, Beijing 100053, China
[9]These authors contributed equally
[10]Lead contact
*Correspondence: zhouying2018@whu.edu.cn (Y.Z.), dr.liangwei@whu.edu.cn (W.L.), yuncao1223@hainmc.edu.cn (Y.C.)
https://doi.org/10.1016/j.xcrm.2024.101690

SUMMARY

Hyperuricemic nephropathy (HN) is a global metabolic disorder characterized by uric acid (UA) metabolism dysfunction, resulting in hyperuricemia (HUA) and tubulointerstitial fibrosis (TIF). Sodium-dependent glucose transporter 2 inhibitor, dapagliflozin, has shown potential in reducing serum UA levels in patients with chronic kidney disease (CKD), though its protective effects against HN remain uncertain. This study investigates the functional, pathological, and molecular changes in HN through histological, biochemical, and transcriptomic analyses in patients, HN mice, and UA-stimulated HK-2 cells. Findings indicate UA-induced tubular dysfunction and fibrotic activation, which dapagliflozin significantly mitigates. Transcriptomic analysis identifies estrogen-related receptor α (ERRα), a downregulated transcription factor in HN. ERRα knockin mice and ERRα-overexpressed HK-2 cells demonstrate UA resistance, while ERRα inhibition exacerbates UA effects. Dapagliflozin targets ERRα, activating the ERRα-organic anion transporter 1 (OAT1) axis to enhance UA excretion and reduce TIF. Furthermore, dapagliflozin ameliorates renal fibrosis in non-HN CKD models, underscoring the therapeutic significance of the ERRα-OAT1 axis in HN and CKD.

INTRODUCTION

Uric acid (UA) is primarily synthesized in the liver as a byproduct of purine and nucleotide metabolism.[1] In the kidney, approximately two-thirds of the UA produced is filtered in the glomerulus, and about 95% of it is subsequently reabsorbed in the proximal tubules, with 50% being re-secreted into the tubular lumen.[2] The functioning of this process relies on several UA transporter proteins, including organic anion transporter 1 (OAT1), uric acid transporter 1 (URAT1), glucose transporter 9 (GLUT9), and adenosine triphosphate (ATP)-binding cassette superfamily G member 2 (ABCG2).[3] OAT1 has been identified as a crucial player in UA excretion, and drugs that target OAT1 have demonstrated potential therapeutic value.[4]

Dysregulated expression of transporter proteins inevitably leads to elevated levels of UA, exceeding the physiological range, which in turn triggers apoptosis, inflammation, and oxidative stress in proximal tubular cells, impairing their function.[5] Additionally, damaged proximal tubular cells contribute to the development of tubulointerstitial fibrosis (TIF) by activating autocrine and paracrine pathways.[6] Several studies have identified TIF as a key factor in the progression from hyperuricemia (HUA) to hyperuricemic nephropathy (HN).[7] The global prevalence of both HUA and HN has witnessed a rapid increase in recent decades,[8] resulting in a substantial burden on public health and the economy.[9] Therefore, it is imperative to develop effective strategies for preventing the progression of HN and improving renal function in order to alleviate this burden. Currently, the treatment of HN primarily involves managing symptoms, highlighting the need to explore new drug options for HN improvement.[10]

Dapagliflozin, an sodium-glucose co-transporter 2 (SGLT2) inhibitor, has demonstrated significant clinical efficacy in patients with diabetes and diabetic kidney disease, leading to a notable reduction in the risk of renal deterioration and cardiovascular complications.[11] Mechanistically, dapagliflozin reduces glucose

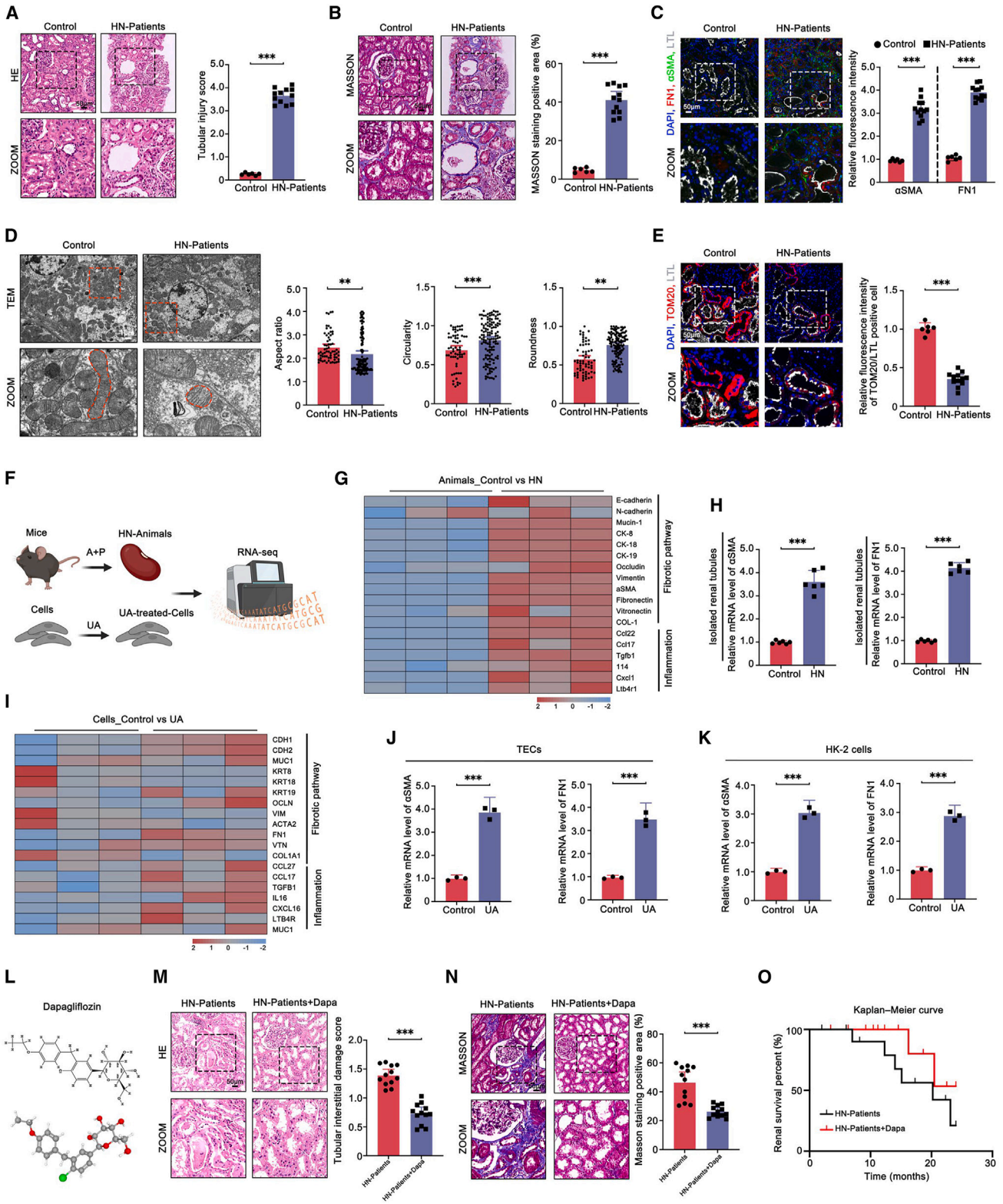

Figure 1. Effects of dapagliflozin on renal fibrosis of patients with HN

(A and B) Representative images of H&E, Masson staining and quantitation of tubular injury score, and Masson staining-positive area in kidney sections from each patient group.

(legend continued on next page)

reabsorption, mitigates inflammation, and attenuates TIF in mice with diabetic nephropathy by selectively inhibiting SGLT2 expression in proximal tubules.[12] Recent studies have also indicated that dapagliflozin may have a role in non-diabetic kidney diseases, including ischemic or hypertensive nephropathy and glomerulonephritis such as IgA nephropathy, focal segmental glomerulosclerosis, and membranous nephropathy.[13] Moreover, dapagliflozin has been shown to diminish UA levels in diabetic model mice,[14] and clinical studies have also corroborated its ability to lower UA levels in patients with heart failure, exerting a protective effect.[15] Despite these findings, the protective effect of dapagliflozin against HN and its specific mechanism have not been elucidated. Therefore, the objective of this study was to explore the protective effect of dapagliflozin against HN and investigate its potential mechanisms.

RESULTS

Dapagliflozin attenuated renal dysfunction and fibrosis in patients with HN

Given that TIF is a common characteristic of HN, we examined kidney specimens of patients with HN to visualize the renal pathological changes. H&E and Masson staining showed severe tubular lesions (including lumen dilation, epithelial vacuolation/flatness, nucleus exposure, and brush border loss) and collagen deposition (Figures 1A and 1B), while immunofluorescence (IF) staining demonstrated the upregulation of the fibrotic markers αSMA and FN1 in the renal tubules of patients with HN (Figure 1C). Furthermore, the renal tubules of patients with HN exhibited mitochondrial morphology abnormalities, structural disruption (such as swelling, vacuole formation, and loss of cristae structure), and depletion, as evidenced by lower aspect ratio, higher circularity and roundness, and reduced TOM20 (mitochondrial marker) fluorescence intensity (Figures 1D and 1E). The baseline characteristics of experimental and control groups that selected HN and control (non-diseased regions adjacent to cancerous tissues) patients, respectively, are presented in Table S1.

Analysis of bulk RNA sequencing (RNA-seq) data from the kidneys of HN mice and cells exposed to UA demonstrated a significant upregulation of fibrotic and inflammatory markers (Figures 1F, 1G, and 1I). Subsequently, quantitative reverse-transcription PCR (qRT-PCR) analyses were conducted using mRNA extracted from isolated renal tubules, tubular epithelial cells (TECs), and HK-2 cells. As anticipated, significantly elevated αSMA and FN1 levels were observed in HN or UA conditions, confirming the activation of the fibrotic pathway (Figures 1H, 1J, and 1K).

Currently, the UA-lowering effect of dapagliflozin, a highly selective SGLT2 inhibitor that shows 2D and 3D chemical structure in Figure 1L, was observed in clinical trials, which may partially explain its long-term renal protective abilities in HN.[16] However, the specific mechanism by which dapagliflozin benefits patients with HN was unclear. We thus assessed renal fibrosis and renal survival percent (a 2-fold increase in serum creatinine [Cr] was set as the endpoint) to evaluate the therapeutic efficacy of dapagliflozin in patients with HN. As illustrated in Figures 1M–1O, dapagliflozin in HN demonstrated anti-fibrotic and renal protective effects. This was evidenced by the attenuation of tubular lesions and collagen deposition in H&E and Masson staining, as well as the renal survival percentage (the increase of serum Cr levels to twice the baseline value). Our findings suggested that investigating the underlying mechanism of dapagliflozin in UA reduction could lead to potential therapeutic targets for HN.

Dapagliflozin reversed functional indices and pathological damage in HN mice

We then established a mouse model of HN by administering adenine (0.16 g/kg) and potassium oxonate (2.4 g/kg) every other day via oral gavage for 4 weeks (Figure 2A). Consistent with the observations in patients with HN, HN mice displayed significant alterations in renal functional parameters and histopathology. These changes were evidenced by elevated levels of serum UA, Cr, and blood urea nitrogen (BUN) (Figure 2B), as well as severe tubular injury (Figure 2C), fibrosis (Figure 2F), and extensive renal interstitial collagen accumulation (Figures 2D and 2E).

To assess the impact of dapagliflozin on HN mice, we developed a model of dapagliflozin-treated HN mice at a dosage of 1.0 mg/kg (Figure 2G). As anticipated, the HN + dapagliflozin group exhibited lower serum UA, Cr, and BUN levels than the HN group (Figures 2H–2J). Dapagliflozin also effectively ameliorated the pathological damage in HN mice, as revealed by the H&E staining-analyzed tubular injury score, as well as the positive area measured from Masson and Sirius Red staining

(C) Representative images of αSMA (green), FN1 (red), and LTL (white) immunofluorescent staining and quantitation of αSMA and FN1 fluorescence intensity in kidney sections from each patient group.
(D) Representative TEM images of mitochondria and quantitation of aspect ratio, circularity, and roundness in kidney sections from each patient group. Red outlines indicate mitochondria.
(E) Representative images of TOM20 (red) and LTL (white) immunofluorescent staining and quantitation of TOM20 fluorescence intensity in kidney sections from each patient group.
(F) Schematic diagram of the RNA-seq using kidneys from HN-animals, UA-treated cells.
(G and I) Heatmap showing the upregulation of fibrotic pathway and inflammation in kidneys from HN mice (GEO: GSE190205) or UA-treated cells (GEO: GSE198133) versus the control group.
(H, J, and K) Representative quantitation of αSMA and FN1 mRNA levels normalized to β-actin in isolated renal tubules, TECs, or HK-2 cells per group.
(L) Chemical structure formula of dapagliflozin in 2D and 3D conformer.
(M and N) Representative images of H&E, Masson staining and quantitation of tubular injury score, and Masson staining-positive area in kidney sections from each patient group.
(O) Renal survival percent (an increase in serum Cr levels to twice the baseline value) (Kaplan-Meier curve) in each patient group over time. Log-rank test $p < 0.001$. A, adenine; P, potassium oxonate; Dapa, dapagliflozin. control patients ($N = 6$), patients with HN ($N = 12$), and patients with HN + Dapa ($N = 12$); $n = 3$ cultures per group; ns: not significant ($p > 0.05$), *$p < 0.05$, **$p < 0.01$, ***$p < 0.001$; five visual fields for each section analyzed.

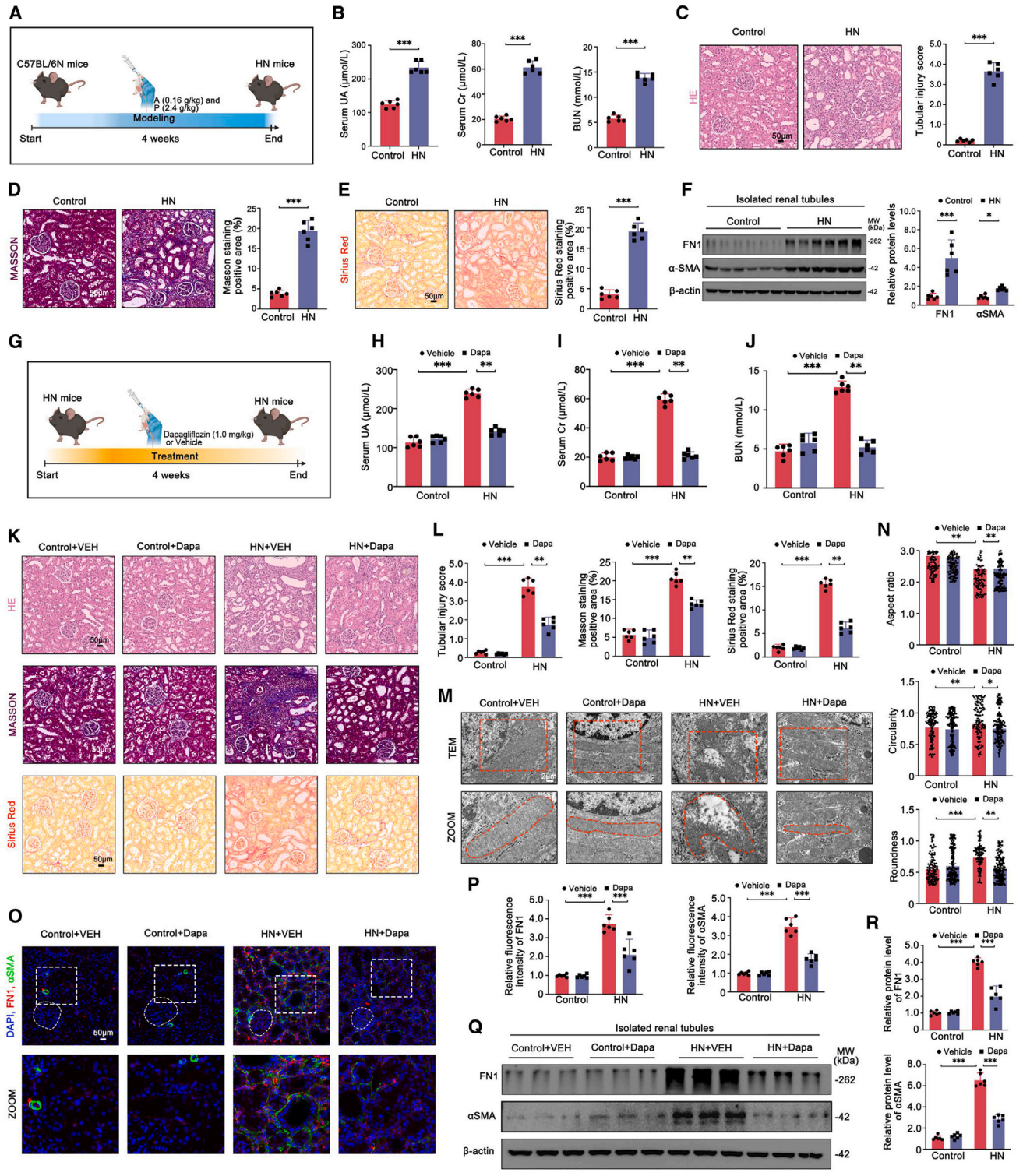

Figure 2. Effects of dapagliflozin on renal fibrosis of HN mice

(A) Schematic diagram of the HN mice model construction.

(B) Serum UA, Cr, and BUN levels in each mouse group.

(C–E) Representative images of H&E, Masson, and Sirius Red staining, and quantitation of tubular injury score, Masson staining-positive area, and Sirius Red staining-positive area in kidney sections from each mouse group.

(F) Representative western blots of αSMA, FN1 protein and quantification of protein levels normalized to β-actin in isolated renal tubules from each mouse group.

(legend continued on next page)

(Figures 2K and 2L). Furthermore, transmission electron microscope (TEM) analysis demonstrated that dapagliflozin substantially mitigated the morphological and structural abnormalities of mitochondria (Figures 2M and 2N). Fibrotic markers, namely αSMA and FN1, were also downregulated in the TECs of dapagliflozin-treated HN mice (Figures 2O–2R).

In order to evaluate the impact of dapagliflozin comprehensively, an additional HN group was included, treated with the first-line UA-lowering drug, allopurinol, at a dosage of 5.0 mg/kg (Figure S1A). As illustrated in Figures S1B–S1J, the renal function and histopathology of HN + dapagliflozin mice exhibited a comparable trend to that of HN + allopurinol (ALL) mice, when compared to HN mice. Consequently, our findings demonstrated that dapagliflozin effectively alleviated renal dysfunction and fibrosis in HN mice. Furthermore, they provided a comparative perspective, indicating that the mechanism behind dapagliflozin's therapeutic effects in HN may not be identical to allopurinol.

Dapagliflozin restored ERRα expression in HN mice and patients with HN

Genome-wide association studies have revealed a close association between the incidence of HUA and genetic polymorphisms in the genes responsible for urate transporter expression.[17] These transporters, on behalf of GLUT9, URAT1, OAT1, NPT1, ABCG2, and MRP4, play a crucial role in the absorption or excretion of urate in the renal proximal tubules (Figure S2A). By analyzing renal RNA-seq data from mice, a volcano plot was generated to summarize a large number of differentially expressed genes (DEGs) with $|Log2FC| > 2$ changes in abundance (Figure S2B). The heatmap further illustrated the dysregulated expression of two types of transporters that resulted in urate accumulation (Figure S2C).

Recent studies have emphasized the importance of transcriptional regulation of urate transporters in maintaining serum UA homeostasis.[18] Consistently, gene ontology enrichment analysis revealed that genes involved in DNA-binding transcription factor (TF) binding play crucial roles in the biological process of HN (Figure S2D). Consequently, we examined the profiles of renal DNA-binding TFs and observed a significant deficiency of estrogen-related receptor α (ERRα) in HN mice, while other TFs were upregulated, suggesting a role for ERRα deficiency in HN (Figure S2E). ERRα has been recognized as a master TF that drives metabolic changes associated with the severity of kidney disease.[19] The qRT-PCR analysis further confirmed decreased mRNA levels of ERRα in HN or UA conditions (Figures S2F and S2G). Our analysis of single-nucleus RNA-seq data from the Kidney Precision Medicine Project website also confirmed parallel trends of ERRα-positive TECs in patients with chronic kidney disease (CKD) to HN mice (Figure S2H; and Table S4). Moreover, immunohistochemistry (IHC) and IF staining using kidney specimens of patients with HN and HN mouse models showed reduced ERRα expression, while dapagliflozin markedly reversed it (Figures S2I–S2L). These findings highlighted the potential role of the DNA-binding TF, ERRα. ERRα deficiency may facilitate the progression of HN by regulating the transcription of urate transporters. More importantly, dapagliflozin may mitigate HN by restoring ERRa expression.

Dapagliflozin activated ERRα to protect against UA-induced injury of TECs and HK-2 cells

We conducted a series of *in vitro* experiments to elucidate the mechanism through which dapagliflozin exerts its potent therapeutic effect in HN. A CCK-8 agent was first utilized to determine the optimal concentration of dapagliflozin (10 μM) that maintained HK-2 cells' viability with 400 μM UA (Figure S3A). Then, TECs and HK-2 cells were divided into four subsets: control, control + dapaglifozin, UA, and UA + dapaglifozin. In accord with the *in vivo* observations, western blot (WB) and IF analyses indicated that dapagliflozin treatment reduced UA-induced fibrotic changes in TECs and HK-2 cells, which interestingly contrasted with the uptrend of ERRα protein expression (Figures 3A–3C and S3B–S3D). Furthermore, the mitochondrial morphology observed post-dapagliflozin treatment was distinct from that observed in the untreated control group. In the treated group, elongated, tubular, and intact mitochondria were observed, in contrast to the round, small, and swollen mitochondria that were abundant in the untreated control group (Figures 3D and 3E, S3E and S3F). Further investigation revealed that dapagliflozin exerts a beneficial effect on mitochondrial function, as evidenced by the observed improvement in oxygen consumption rate (OCR), ATP levels, and mitochondrial morphology, as well as a reduction in reactive oxygen species (ROS) production in TECs stimulated with UA (Figures 3F–3I).

In view of the potential mediation of dapagliflozin on ERRα, molecular protein docking analysis was conducted and revealed a robust binding interaction between dapagliflozin and ERRα (Figure 3J). To further investigate whether ERRα is a direct target of dapagliflozin, cellular thermal shift assay (CETSA) and drug affinity responsive target stability (DARTS) assays were employed. As shown in Figures S3G and S3I, exposure to dapagliflozin resulted in increased thermal stability of ERRα in cell lysate

(G) Schematic diagram of the HN mice with dapagliflozin treatment.
(H–J) Serum UA, Cr, and BUN levels in each mouse group.
(K and L) Representative images of H&E, Masson, and Sirius Red staining, and quantitation of tubular injury score, Masson staining-positive area, and Sirius Red staining-positive area in kidney sections from each mouse group.
(M and N) Representative TEM images of mitochondria and quantitation of aspect ratio, circularity, and roundness in kidney sections from each mouse group. Red outlines indicate mitochondria.
(O and P) Representative images of αSMA (green), FN1 (red) immunofluorescent staining and quantitation of fluorescence intensity in kidney sections from each mouse group. White circle represents glomeruli.
(Q and R) Representative western blots of αSMA, FN1 protein and quantification of protein levels normalized to β-actin in isolated renal tubules from each mouse group. VEH, vehicle; A, adenine; P, potassium oxonate; Dapa, dapagliflozin; $n = 6$ independent group mice; ns: not significant ($p > 0.05$), $^{*}p < 0.05$, $^{**}p < 0.01$, $^{***}p < 0.001$; five visual fields for each section analyzed.

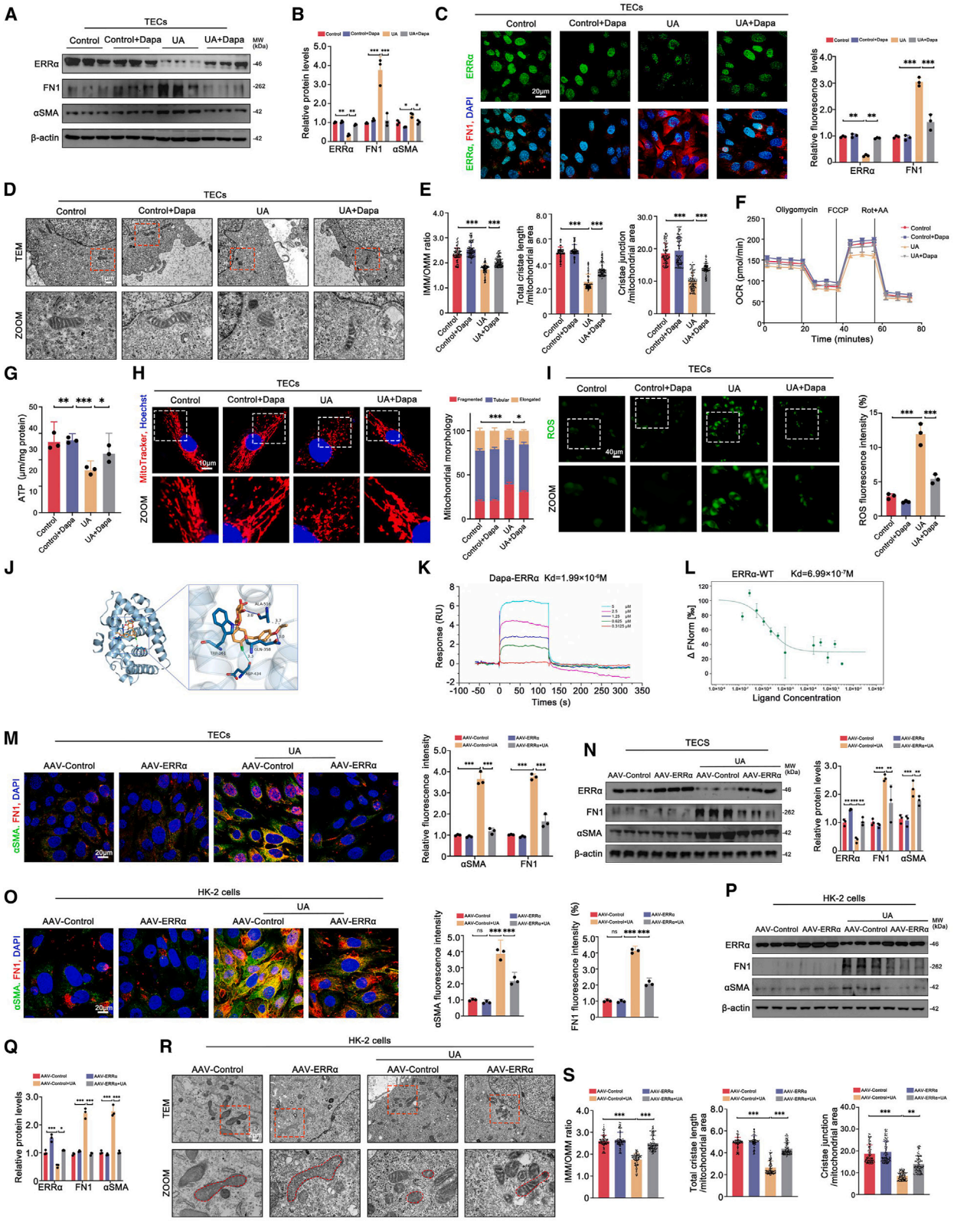

(legend on next page)

compared to the control treated with DMSO. The interaction of dapagliflozin with ERRα resulted in enhanced resistance to protease digestion (Figures S3H and S3J), indicating that dapagliflozin may target the ERRα protein. Furthermore, surface plasmon resonance and microscale thermophoresis analysis demonstrated a robust affinity between dapagliflozin and the ERRα protein, with an affinity constant of 1.99×10^{-6} M and 6.99×10^{-7} M (Figures 3K and 3L).

Building upon the aforementioned findings regarding the beneficial impact of upregulating ERRα, we proceeded to transfect adeno-associated virus ERRα (AAV-ERRα), investigating whether it could protect against UA-induced injury in TECs and HK-2 cells. In line with dapagliflozin treatment, ERRα overexpression resulted in a significant reduction in the fluorescence and grayscale of αSMA and FN1 in two types of UA-exposed cells, suggesting a resultful anti-fibrotic effect (Figures 3M–3Q); TEM analysis also revealed marked repair in the mitochondria damage in the UA + AAV-ERRα group (Figures 3R and 3S). Together, these findings highlighted the regulatory mechanism underlying the damage-resistant and anti-fibrotic actions of dapagliflozin in UA-exposed TECs and HK-2 cells through targeting ERRα.

Dapagliflozin had no effect on UA-induced HK-2 cell injury under ERRα depletion or inhibition

Given that ERRα in tubules could be closely associated with the protective effect of dapagliflozin for HN, which traditional attitudes suggest is based on SGLT2 inhibition, the SGLT2-knockout (KO) cell line was thus established by HK-2 cells using CRISPR-Cas9 to probe deeper into it (Figure 4A). It was observed that dapagliflozin significantly protected against UA-induced fibrosis and mitochondrial dysfunction, despite SGLT2 depletion. This suggests that the protective mechanism of dapagliflozin for HN may be independent of SGLT2 inhibition (Figures 4B–4G). Moreover, SGLT2 depletion did not affect ERRα expression (Figures 4B and 4C).

Afterward, additional *in vitro* experiments were carried out to test whether ERRα depletion or inhibition could intensify UA-induced effects in HK-2 cells. The ERRα-KO cell line was successfully established (Figure 4H). As demonstrated by WB, IF, and OCR analyses, ERRα depletion resulted in a shift in UA-induced HK-2 cell injury toward a more severe state (Figures 4I–4M). Notably, in contrast to the SGLT2-KO cell line, dapagliflozin was ineffective in preventing UA-induced fibrosis and mitochondrial dysfunction in the ERRα-KO cell line. This was evidenced by the persistence of fibrotic marker upregulation, ROS overgeneration, mitochondrial fragmentation, and OCR and ATP reduction (Figures 4I–4N). XCT-790 (compound 12) is a potent and selective ERRα reverse agonist.[20] The molecular protein docking technique was applied and displayed the forceful binding affinity of XCT-790 and ERRα protein (Figure S4A). Parallel to ERRα depletion, XCT-790 inhibited ERRα levels and enhanced FN1, αSMA expression, leading to swelling and shortening of mitochondria, which were exacerbated than simple UA conditions, even under dapagliflozin treatment (Figures S4B–S4E). In short, these findings further supported our supposition, indicating ERRα is a downstream target of dapagliflozin independent of SGLT2. Tubular cells subjected to ERRα depletion or inhibition were more susceptible to UA stimulation.

Tubule-specific ERRα overexpression alleviated renal dysfunction and fibrosis in HN mice

To investigate the direct association between ERRα and the development of HN, we generated tubule-specific ERRα overexpression ($ERR\alpha^{ptKI}$) mice (Figure 5A). PCR analysis confirmed the genotype of $ERR\alpha^{Control}$ mice (Figure 5B, lane 1–4 and 6) and $ERR\alpha^{ptKI}$ mice (Figure 5B, lane 5). Furthermore, WB analysis verified the efficient knockin of ERRα (Figures 5C and 5D). In terms of renal functional indices, $ERR\alpha^{ptKI}$ mice did not exhibit noticeable changes compared to $ERR\alpha^{Control}$ mice, but after HN modeling, $ERR\alpha^{ptKI}$ mice showed significant relief compared to $ERR\alpha^{Control}$ mice (Figures 5E–5H). These findings were consistent with a visible alleviation of pathological alterations, such as collagen accumulation, tubular lesions, and mitochondrial damage in the kidneys of HN-modeled $ERR\alpha^{ptKI}$ mice (Figures 5I–5N). Moreover, the reduced fluorescence and grayscale of αSMA and FN1 further confirmed the suppressive effects of ERRα's genetic overexpression on renal fibrosis in HN mice (Figures 5O

Figure 3. Effects of dapagliflozin or ERRα overexpression in UA-treated TECs and HK-2 cells

(A and B) Representative western blots of ERRα, αSMA, and FN1 protein and quantification of protein levels normalized to β-actin in each TEC group.

(C) Representative images of ERRα (green) and FN1 (red) immunofluorescent staining and quantitation of fluorescence intensity in each TEC group.

(D and E) Representative TEM images of mitochondria and quantitation of inner mitochondrial membrane (IMM)/outer mitochondrial membrane (OMM) ratio, total cristae length/mitochondrial area, and cristae junction/mitochondrial area in each TEC group. Red outlines indicate the zoom area.

(F) Representative traces show OCR in each TEC group.

(G) Representative quantitation of ATP levels in each TEC group.

(H) Representative images of MitoTracker (red) immunofluorescent staining and quantitation of mitochondrial morphology in each TEC group. White outlines indicate the zoom area.

(I) Representative images of ROS (green) immunofluorescent staining and quantitation of fluorescence intensity in each TEC group.

(J) Diagram of the spatial binding pattern of dapagliflozin and ERRα protein.

(K) Dapagliflozin's bond with ERRα analyzed by surface plasmon resonance (SPR).

(L) Dapagliflozin's bond with ERRα analyzed by microscale thermophoresis (MST).

(M and O) Representative images of αSMA (green) and FN1 (red) immunofluorescent staining and quantitation of fluorescence intensity in each TEC and HK-2 cell group.

(N, P, and Q) Representative western blots of ERRα, αSMA, and FN1 protein and quantification of protein levels normalized to β-actin in each TEC and HK-2 cell group.

(R and S) Representative TEM images of mitochondria and quantitation of IMM/OMM ratio, total cristae length/mitochondrial area, and cristae junction/mitochondrial area in each HK-2 cell group. Red outlines indicate the zoom area and mitochondria. Dapa, dapagliflozin; n = 3 cultures per group; MitoTracker, mitochondrial marker; Hoechst, nucleus marker; ns: not significant ($p > 0.05$), $^{*}p < 0.05$, $^{**}p < 0.01$, $^{***}p < 0.001$; five visual fields for each section analyzed.

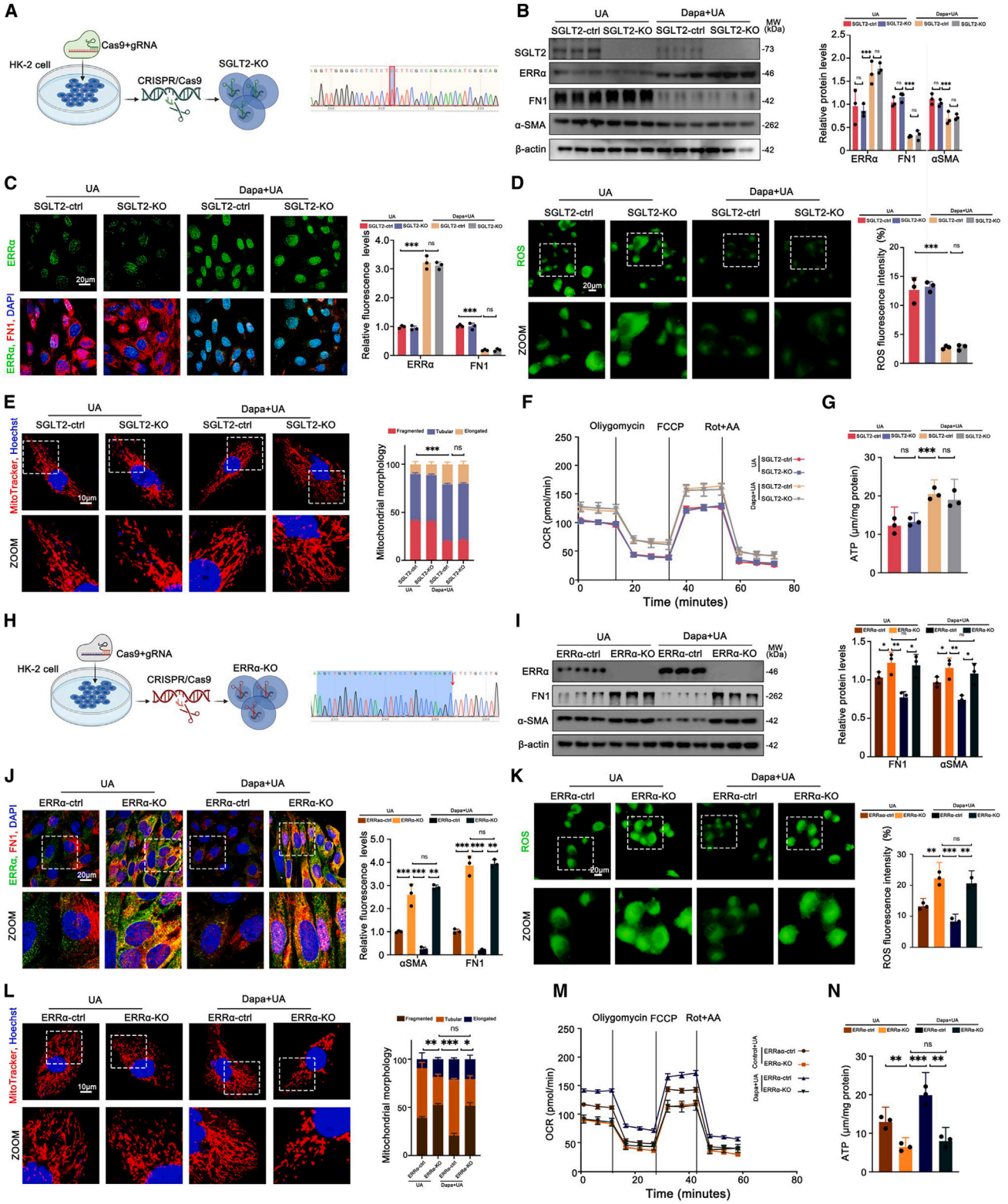

(legend on next page)

and 5P). Collectively, these results emphasized the therapeutic significance of ERRα in the treatment of HN.

ERRα bound to OAT1 for transcriptional regulation

OAT1 (SLC22A6/NKT) is a multispecific transporter mainly located on the basolateral membrane of the kidney proximal tubule. It plays a crucial role in actively secreting a wide range of endogenous and exogenous substances, including urate.[21] OAT1 dysregulation has been shown to disrupt UA metabolism and increase the risk of HUA.[4] Recent studies have indicated that estrogen receptor α (ERα) indirectly activates OAT1, suggesting that its activity is partially regulated by estrogen-dependent transcriptional mechanisms.[22] The chord diagram (Figure 6A) depicted the differential pathways in small interfering (si)-ERRα--transfected HK-2 cells versus controls, including tyrosine metabolism, serotonergic synapse, nicotinate and nicotinamide metabolism, Wnt signaling pathway, transforming growth factor β (TGF-β) signaling pathway, and tumor necrosis factor signaling pathway. These pathways have previously been reported to be closely associated with the pathogenesis of HUA.[23,24] Given the potential connection between ERRα and OAT1 in HN, we employed various validation methods to determine if ERRα directly regulates OAT1 activity at the transcriptional level. Our chromatin immunoprecipitation sequencing (ChIP-seq) analysis in HK-2 cells (Figure 6B) identified the binding site of the OAT1 gene with ERRα protein, which was further supported by the subsequent agarose gel image, showing ERRα protein enrichment on OAT1 gene fragments (Figure 6C). To predict the complementary sequence of the ERRα-targeted motif in the promoter region of the OAT1 gene, the JASPAR database was searched. The sequence "TCAAGGTCA" (5′→3′, score 9.275842) was predicted as the ERRα-targeted motif in the OAT1 gene (Figure 6D). Protein-DNA docking simulations revealed the best matching pattern between the ERRα protein and the OAT1 gene (Figure 6E).

Furthermore, at the mRNA and protein level, overexpression of ERRα by AAV-ERRα 24 h after si-ERRα transfection in both TECs and HK-2 cells was observed to rescue OAT1 levels, while si-ERRα was found to downregulate OAT1 expression (Figures 6F and 6G). Subsequently, a dual-luciferase reporter assay established pcDNA3.1-NC, pcDNA3.1-ERRα, OAT1-wild-type (WT), and OAT1-MUT (double-strand mutation, 5′→3′, "TATGACGTTGGTC" mutated into "CGCAGTACCAACT") plasmids, to confirm the interaction between ERRα and the predicted motif in the promoter region of the OAT1 gene, as evidenced by the significant increase in bioluminescence in the OE-ERRα + OAT1-WT group, while the overexpression of ERRα (OE-ERRα) + OAT1-MUT group showed no effect (Figure 6H). Furthermore, WB analysis provided further support for the regulatory role of ERRα on OAT1 in both TECs and HK-2 cells, demonstrating the pronounced inhibition of OAT1 bands in the presence of si-ERRα, even when the OAT1-WT plasmid was transfected. This inhibition was not observed when the OAT1-MUT plasmid was utilized (Figures 6I and 6J). Overall, these findings highlighted the transcriptional regulatory efficacy of ERRα on OAT1.

Dapagliflozin ameliorated fibrotic changes in HN kidneys and UA-treated tubular cells by activating the ERRα-OAT1 axis

It was postulated that an enhanced ERRα-OAT1 axis could account for the favorable effects of dapagliflozin on HN, given that the expression of OAT1 protein exhibited a negative correlation with functional parameters such as serum UA ($r = -0.5895$, $p = 0.043$) and BUN ($r = -0.7067$, $p = 0.010$) in patients with HN without dapagliflozin treatment, despite no significant correlation with serum Cr ($r = -0.5365$, $p = 0.072$) and urinary albumin to creatinine ratio (UACR) ($r = -0.4635$, $p = 0.1291$) (Figures 7B–7E). Consistent with previous studies, we observed a distinct decrease in the number of OAT1-positive cells in the proximal tubules of patients with HN (Figure 7A). IF staining also confirmed the reduced fluorescence of OAT1 in patients with HN (Figure 7F). Nevertheless, dapagliflozin treatment was found to reverse OATI expression (Figures 7A and 7F). Additionally, our evaluation of mice, TECs, and HK-2 cells under HN or UA conditions revealed a downregulation of OAT1 protein levels, which was countered by dapagliflozin treatment (Figures 7G–7K). Behind, OE-OAT1 was transfected into TECs and HK-2 cells and validated the negative impacts of OAT1 on UA-caused fibrotic changes, which were characterized by upregulation of FN1 and αSMA (Figures 7L–7O). However, OAT1 overexpression did not alter ERRα protein levels (Figures S5A and S5B). Together, our data confirmed the pivotal application of dapagliflozin to protect against renal fibrosis in HN by targeting the ERRα-OAT1 axis, supporting the notion of HN as a disease that could be effectively addressed by dapagliflozin.

Dapagliflozin mitigated fibrotic changes in non-HN CKD mouse models and high-glucose- or TGF-β-treated TEC models

The aforementioned results indicate that the activated ERRα-OAT1 axis may be a mechanism by which dapagliflozin

Figure 4. Effects of dapagliflozin in UA-treated SGLT2- or ERRα-KO HK-2 cells

(A and H) Diagram of the SGLT2 or ERRα gene KO by CRISPR-Cas9 technology and sequencing identification in HK-2 cells.

(B and I) Representative western blots of SGLT2, ERRα, αSMA, and FN1 protein and quantification of ERRα, αSMA, and FN1 protein levels normalized to β-actin in each HK-2 cell group.

(C and J) Representative images of ERRα (green) and FN1 (red) immunofluorescent staining and quantitation of fluorescence intensity in each HK-2 cell group. White outlines indicate the zoom area.

(D and K) Representative images of ROS (green) immunofluorescent staining and quantitation of fluorescence intensity in each HK-2 cell group. White outlines indicate the zoom area.

(E and L) Representative images of MitoTracker (red) immunofluorescent staining and quantitation of mitochondrial morphology in each HK-2 cell group. White outlines indicate the zoom area.

(F and M) Representative traces show OCR in each HK-2 cell group.

(G and N) Representative quantitation of ATP level in each HK-2 cell group. Dapa, dapagliflozin; $n = 3$ cultures per group; MitoTracker, mitochondrial marker; Hoechst, nucleus marker; ns: not significant ($p > 0.05$), *$p < 0.05$, **$p < 0.01$, ***$p < 0.001$; five visual fields for each section analyzed.

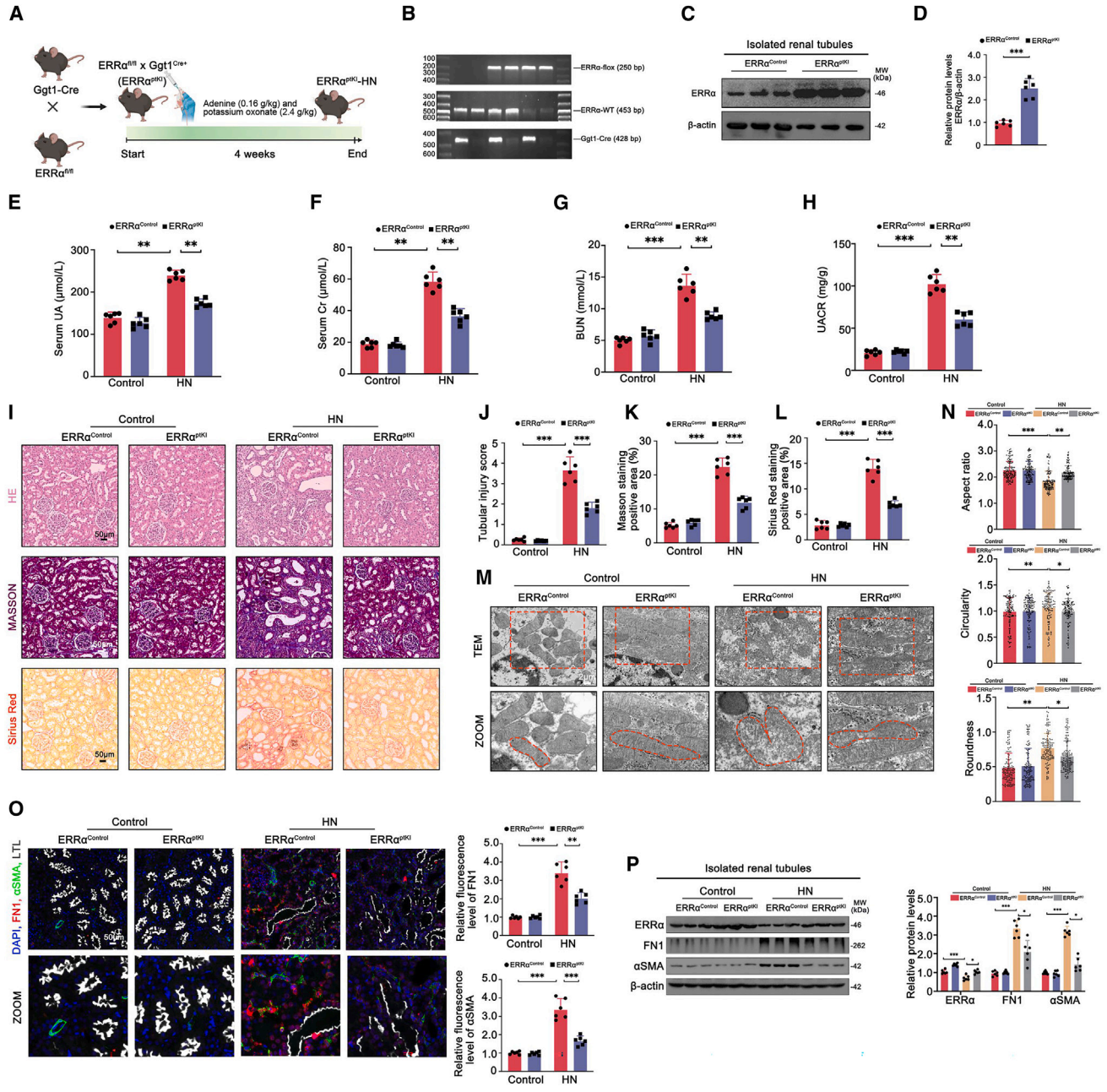

Figure 5. Effects of tubule-specific ERRα overexpression in HN mice

(A) Schematic diagram of the ERRα^{ptKI} mice generation and subsequent HN mice model construction.

(B) Genotyping the mice by PCR analysis of genomic DNA; lanes 1–4 and 6 are ERRα^{Control} genotype and lane 5 is ERRα^{ptKI} genotype.

(C and D) Representative western blots of ERRα protein and quantification of protein level normalized to β-actin in isolated renal tubules from each mouse group.

(E–H) Serum UA, Cr, BUN, and UACR levels in each mouse group.

(I, J, K, and L) Representative images of H&E, Masson, and Sirius Red staining and quantification of tubular injury score, Masson staining=positive area, and Sirius Red staining-positive area in kidney sections from each mouse group.

(M and N) Representative TEM images of mitochondria and quantitation of aspect ratio, circularity, and roundness in kidney sections from each mouse group. Red outlines indicate the zoom area and mitochondria.

(O) Representative images of αSMA (green), FN1 (red), and LTL (white) immunofluorescent staining and quantitation of αSMA and FN1 fluorescence intensity in kidney sections from each mouse group.

(P) Representative western blots of ERRα, FN1, and αSMA protein and quantification of protein levels normalized to β-actin in isolated renal tubules from each mouse group. n = 6 independent group mice; ns: not significant ($p > 0.05$), *$p < 0.05$, **$p < 0.01$, ***$p < 0.001$; five visual fields for each section analyzed.

CellPress
OPEN ACCESS

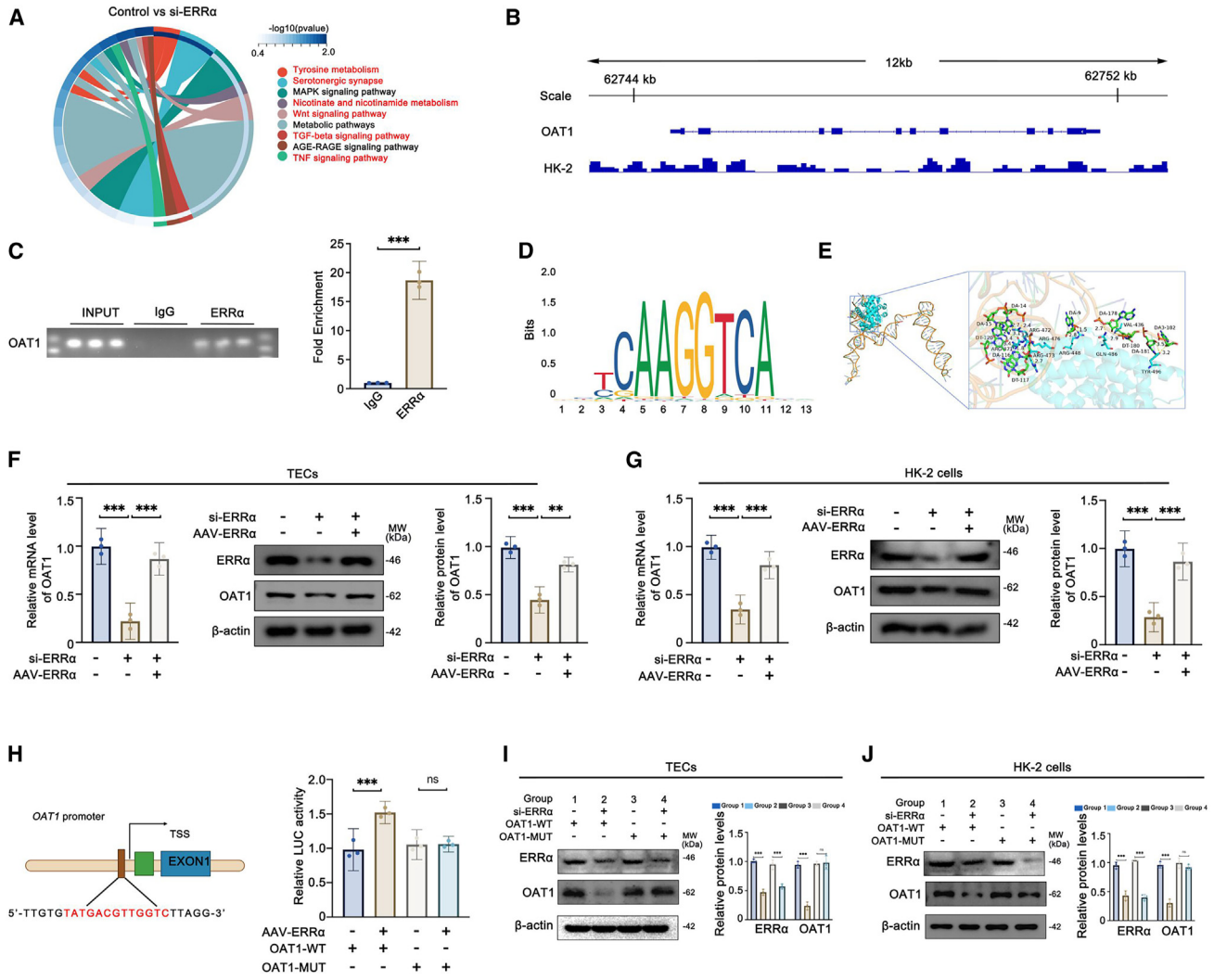

Figure 6. ERRα-OAT1 axis in HK-2 cells

(A) Chord plots showing KEGG-enriched items of DEGs from HK-2 cells of the control group versus the si-ERRα group.

(B) ChIP-seq analysis: the binding site of OAT1 with ERRα in HK-2 cells.

(C) ChIP-qPCR analysis: representative agarose gel image showing OAT1 gene fragments enrichment on ERRα protein.

(D) Motif analysis: the complementary sequence of the ERRα-targeted motif.

(E) Diagram of the spatial binding pattern of ERRα protein and OAT1 gene.

(F and G) Representative quantitation of OAT1 mRNA and protein levels normalized to β-actin, representative western blots of ERRα and OAT1 protein, and quantification of protein levels normalized to β-actin in each TEC and HK-2 cell group.

(H) Schematic diagram showing the location of the ERRα-targeted motif (in the OAT1 gene's promoter region) when inserted upstream of the luciferase gene. Dual-luciferase reporter assay: relative luciferase activity in each group of HK-2 cells.

(I and J) Representative western blots of ERRα and OAT1 protein and quantification of protein levels normalized to β-actin in each TEC and HK-2 cell group. $n = 3$ cultures per group; ns: not significant ($p > 0.05$), *$p < 0.05$, **$p < 0.01$, ***$p < 0.001$.

benefits patients with HN. HUA is a common phenomenon in patients with CKD.[25] At present, dapagliflozin has been approved for clinical treatment of CKD.[26,27] Nevertheless, the relationship between dapagliflozin's therapeutic effect on CKD and the ERRα-OAT1 axis remains a topic worthy of further investigation. In order to construct non-HN CKD mouse models, we employed three different approaches: high-fat diet (HFD)-induced obesity mice, db/db type 2 diabetic kidney disease (DKD) mice, and unilateral ureteral obstruction (UUO) mice. Subsequently, a 4-week course of dapagliflozin treatment was administered to assess its impact on renal functional indices and pathological damage (Figures S6A, S6F, and S7A). In the three non-HN CKD mouse models, we demonstrated that dapagliflozin could lower serum UA, Cr, and BUN, as well as attenuate tubular lesions and collagen deposition (Figures S6B–S6E, S6G–S6J, and S7B–S7E). It is evident that the enhanced ERRα-OAT1 axis was identified by WB analysis (Figures S6E, S6J, and S7E). Furthermore, *in vitro* simulation of type 2 DKD and UUO mice was conducted

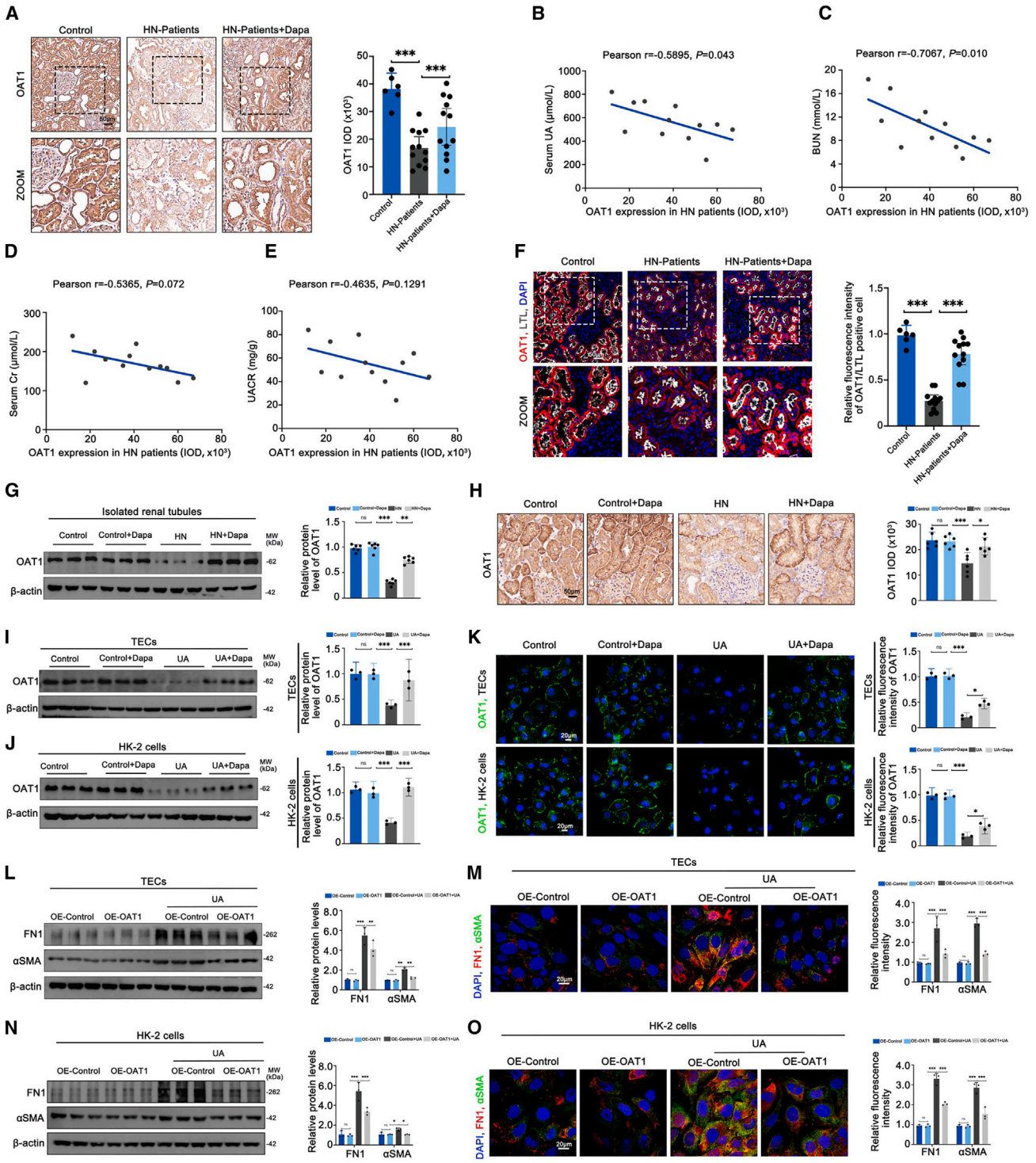

Figure 7. Effects of dapagliflozin on OAT1 expression in tubular cells under HN or UA conditions

(A) Representative IHC images of OAT1 and quantitation of OAT1 integrated option density (IOD) in kidney sections from each patient group.

(B–E) Correlation between tubular OAT1 expression and serum UA, Cr, BUN, and UACR levels in patients with HN without dapagliflozin treatment.

(F) Representative images of OAT1 (red) and LTL (white) immunofluorescent staining and quantification of OAT1 fluorescence intensity in kidney sections from each patient group.

(G) Representative western blots of OAT1 protein and quantification of OAT1 protein level normalized to β-actin in isolated renal tubules from each mouse group.

(H) Representative IHC images of OAT1 and quantitation of OAT1 IOD in kidney sections from each mouse group.

(legend continued on next page)

using HK-2 cells treated with high glucose and TGF-β. The results demonstrated a similar trend in ERRα, OAT1, FN1, and αSMA protein expression compared to the *in vivo* results (Figures S7F–S7I). These data expand our findings that dapagliflozin, a reported regulator of the ERRα-OAT1 axis, could also mitigate fibrotic changes in models of non-HN CKD mice and corresponding tubular cells. In conclusion, this study has provided a more comprehensive theoretical basis for the clinical application of dapagliflozin in non-diabetic kidney diseases, offering an insight.

DISCUSSION

In this study, we made the observation that dapagliflozin improved TIF in both patients with HN and HN mouse models through the activation of the ERRα-OAT1 axis. Mechanistically, we discovered that the TF ERRα played a crucial role in the regulation of UA excretion by controlling the expression of the UA transporter protein OAT1 in the proximal renal tubules. Notably, ERRα expression was downregulated in HN, whereas dapagliflozin treatment led to an upregulation of ERRα expression and an increased OAT1, thereby enhancing UA excretion and attenuating TIF. Overall, our study provides an insight into the potential mechanism underlying dapagliflozin's therapeutic effects in HN. Additionally, it offers compelling evidence for the potential use of dapagliflozin in the treatment of non-diabetic kidney diseases.

Elevated levels of UA over a prolonged period can detrimentally impact the function of renal tubular cells, leading to cell shrinkage and promoting apoptosis or transdifferentiation.[28] These impaired renal tubular cells subsequently contribute to renal fibrosis through autocrine or paracrine secretion, thus exacerbating the progression from HUA to HN.[29] Ultimately, the hallmark pathological manifestation of HN is renal fibrosis, characterized by the upregulation of mesenchymal cell products, such as αSMA and FN1.[30] In our study, HN mouse models induced by adenine and potassium oxonate were examined, which exhibited elevated serum UA levels, impaired renal function, pronounced renal inflammation, and fibrosis, thus confirming the reliability of this modeling approach. Furthermore, we observed a significant improvement in TIF in HN mice treated with dapagliflozin, further substantiating the protective effect of dapagliflozin against the development of HN.

The proximal renal tubules are widely recognized for their crucial involvement in ion reabsorption,[31] with transporter proteins on the cell membrane of these tubules being primarily responsible for UA transport within the kidney.[32] Any changes in these transporter proteins can significantly impact UA reabsorption and secretion, consequently resulting in increased UA levels.[33] OAT1, classified as an organic anion transporter protein, primarily facilitates the secretion of UA into the renal tubule lumen during UA metabolism.[34] Schneider's study has demonstrated that upregulation of OAT1 can protect against renal injury following ischemic acute kidney injury.[35] Furthermore, OAT1 has been acknowledged as a vital target for renal drug transport,[36] lipid transport,[37] and the regulation of gut microbes.[35] Given its substantial role in UA metabolism and renal diseases, we investigated the alterations in OAT1 expression in both patients with HN and HN mouse models. Our findings revealed a downregulation of OAT1 expression in both patients with HN and HN mouse models. Notably, the expression of OAT1 exhibited a correlation with clinical indicators of patients with HN, thus emphasizing OAT1 as an important potential therapeutic target for HN.

OAT1, also known as SLC22A6, belongs to the solute carrier family of transporter proteins,[38] a group regulated by TFs, such as Sirt6,[39] HIF-1α,[40] and Nrf2,[41] under physiological conditions.[42] Earlier studies have highlighted the transcriptional regulation of OAT1 by various nuclear TFs. Sequencing analysis of the OAT1 promoter region identified binding sites for TFs such as PAX1, PBX, WT1, and HNF1.[43] Ligand-activated ERα has been demonstrated to activate CCAAT-box binding TF and heterogeneous nuclear ribonucleoprotein K, both capable of binding to the OAT1 promoter and enhancing its transcription.[22] In our study, utilizing ChIP-seq and dual-luciferase assays, we made the discovery that nuclear TFs, specifically ERRα, could bind to OAT1 and stimulate its transcription. ERRα, classified as a nuclear TF, plays vital roles in maintaining mitochondrial function and fatty acid oxidation and is significantly downregulated in metabolic disorders.[44] Within the kidney, ERRα is predominantly expressed in the proximal renal tubules and has been shown to be downregulated in various conditions, including renal fibrosis,[45] aging,[46] acute kidney injury,[47] and high-salt diet mouse models.[48] The dysregulation of UA metabolism is widely recognized as a significant factor in the development and progression of HN, positioning HN as the fourth most prevalent metabolic disorder following hypertension, hyperlipidemia, and hyperglycemia.[49] Additionally, our study discovered downregulation of ERRα expression in both patients with HN and HN mouse models, indicating inhibition of the transcriptional pathway involved in OAT1 regulation. This disruption influenced UA metabolism and contributed to the progression of HN, further underscoring the importance of ERRα in maintaining UA metabolism within the context of HN as a metabolic disorder.

In recent years, the SGLT2 inhibitor dapagliflozin has demonstrated substantial clinical benefits in the prevention and treatment of diabetes mellitus and DKD. This is achieved by targeting and inhibiting the expression of proximal tubular SGLT2, which in turn reduces sodium and glucose reabsorption. As a result, this ameliorates a wide range of cellular injuries and mitigates the

(I and J) Representative western blots of OAT1 protein and quantification of OAT1 protein level normalized to β-actin in each TEC and HK-2 cell group.
(K) Representative images of OAT1 (green) and quantitation of fluorescence intensity in each TEC and HK-2 cell group.
(L and N) Representative western blots of αSMA and FN1 protein and quantification of protein levels normalized to β-actin in each TEC and HK-2 cell group.
(M and O) Representative images of αSMA (green) and FN1 (red) immunofluorescent staining and quantitation of αSMA and FN1 fluorescence intensity in each TEC and HK-2 cell group. Dapa, dapagliflozin; control patients ($N = 6$), patients with HN ($N = 12$), and patients with HN + Dapa ($N = 12$); $n = 6$ independent group mice; $n = 3$ cultures per group; ns: not significant ($p > 0.05$), $^{*}p < 0.05$, $^{**}p < 0.01$, $^{***}p < 0.001$; five visual fields for each section analyzed.

symptoms of diabetes mellitus and DKD.[11,12] Furthermore, dapagliflozin's potential role in treating non-diabetic diseases is gaining attention. Notably, studies have indicated its positive impact on renal diseases such as hypertensive nephropathy and glomerulonephritis, including IgA nephropathy, focal segmental glomerulosclerosis, and membranous nephropathy. It has been shown to delay the increase in blood creatinine levels in patients and improve prognosis.[13] Although recent clinical studies have suggested dapagliflozin's protective effect against HUA, the exact mechanism and its protective benefits have not been extensively explored.[50] Our research investigated the effect of dapagliflozin on HN in both human patients and mouse models. In this study, we discovered that dapagliflozin significantly ameliorated TIF in patients with HN and HN mice. Through molecular docking, CETSA, and DARTS experiments, we identified that dapagliflozin targets and activates the ERRα to exert its protective effects. Notably, the expression of ERRα was restored after dapagliflozin treatment in both patients with HN and HN mouse models, providing evidence for its potential therapeutic application in non-diabetic renal diseases. Moreover, dapagliflozin effectively restored the downregulated OAT1 in HN, promoting the secretion of UA into the renal tubules. Consequently, this led to a reduction in blood UA levels, further contributing to the protective effects of dapagliflozin. Furthermore, given that renal fibrosis is a common feature of CKD, we also found that dapagliflozin ameliorated TIF through the activation of the ERRα-OAT1 axis in three animal models of non-HN CKD (HFD, UUO, and db/db mice). In conclusion, our findings support the hypothesis that dapagliflozin exerts its protective effects in both HN and non-HN CKD through the upregulation of the ERRα-OAT1 axis.

Limitations of the study

Several limitations of the present study should be considered. Firstly, the overexpression of OAT1 was conducted in an *in vitro* experiment, which promoted uric acid excretion and attenuated renal fibrosis. Future studies that overexpress OAT1 *in vivo* will help to further elucidate the role of OAT1 in HN. Secondly, given the role of ERRα in attenuating renal fibrosis, the targeted agonists of ERRα could be further identified in the future, thereby attenuating the side effects of dapagliflozin. In addition, dapagliflozin may still alleviate renal fibrosis through other mechanisms, such as inhibition of uric acid synthesis or anti-inflammatory mechanisms, and further studies will provide a deeper understanding of the mechanism of action of dapagliflozin.

Conclusion

In conclusion, this study has identified a mechanism through which dapagliflozin facilitates the excretion of UA into the tubular lumen of the renal tubules. This effect is achieved by targeting the ERRα-OAT1 axis, which subsequently results in a reduction in serum UA levels. Notably, this reduction in UA levels plays a pivotal role in the alleviation of TIF in HN and non-HN CKD. The findings of this study contribute insights into the potential treatment of non-diabetic renal diseases using dapagliflozin.

STAR★METHODS

Detailed methods are provided in the online version of this paper and include the following:

- KEY RESOURCES TABLE
- RESOURCE AVAILABILITY
  - Lead contact
  - Materials availability
  - Data and code availability
- EXPERIMENTAL MODEL AND STUDY PARTICIPANT DETAILS
  - Human kidney biopsy specimens and clinical index collection
  - Mouse studies
  - HN mice model construction and treatment
  - ERRα^{ptKI} mice generation and treatment
  - Obesity, type 2 DKD, UUO mice model construction and treatment
  - HK-2 cell culture and treatment
  - SGLT2-or ERRα-KO HK-2 cell line construction and treatment
- METHOD DETAILS
  - Isolation of renal tubules
  - Renal functional parameters measurement
  - Cell viability assay
  - Cell transfection
  - Histological and IHC analysis
  - If assay
  - ROS and ATP analysis
  - OCR detection
  - TEM
  - WB analysis
  - RNA extraction and qRT-PCR analysis
  - Bulk RNA-seq analysis
  - ChIP-seq analysis
  - Dual-luciferase reporter assay
  - GEO dataset and single-nucleus RNA-seq dataset analyses
  - Motif prediction
  - Molecular docking method
  - SPR analysis
  - MST analysis
  - DARTS
  - CETSA
- QUANTIFICATION AND STATISTICAL ANALYSIS

SUPPLEMENTAL INFORMATION

Supplemental information can be found online at https://doi.org/10.1016/j.xcrm.2024.101690.

ACKNOWLEDGMENTS

We are grateful for the technical support for immunofluorescence provided by Hubei BIOSSCI Biotech Co., Ltd (Wuhan Changyan Pathology Technology Co., Ltd). We are grateful for the technical support for SPR and MST assays provided by Yangene Biological (Wuhan Yangene Biological Technology Co., Ltd). We are grateful for single-nucleus RNA-seq data provided by Kidney Interactive Transcriptomics (https://www.humphreyslab.com). This work was supported by grants from the National Natural Science Foundation of China (81970631 to W. Liang and 82360146 to J.W.), Hainan key research and development projects (ZDYF2022SHFZ016), and Hainan Province Clinical Medical Center. The figures were created with BioRender.com.

AUTHOR CONTRIBUTIONS

H.H. designed all the experiments and performed imaging, cell culture, biochemistry, Seahorse experiments, lentivirus production, and data analysis. W. Li performed cell culture and RNA-seq analyses and helped with immunoblots. Y.H. and Z.P. helped with cell culture and experimental design. Y.H., Z.Z., and W. Li helped with the animal experiments. J.W., Y.Z., W. Li, and

Y.C. supervised the project and provided funding. All data were generated in-house. All authors agree to be accountable for all aspects of the work to ensure integrity and accuracy.

DECLARATION OF INTERESTS

The authors declare no competing interests.

Received: January 3, 2024
Revised: July 1, 2024
Accepted: July 24, 2024
Published: August 20, 2024

REFERENCES

1. Crawley, W.T., Jungels, C.G., Stenmark, K.R., and Fini, M.A. (2022). U-shaped association of uric acid to overall-cause mortality and its impact on clinical management of hyperuricemia. Redox Biol. *51*, 102271. https://doi.org/10.1016/j.redox.2022.102271.
2. Mandal, A.K., and Mount, D.B. (2015). The molecular physiology of uric acid homeostasis. Annu. Rev. Physiol. *77*, 323–345. https://doi.org/10.1146/annurev-physiol-021113-170343.
3. Adomako, E.A., and Moe, O.W. (2023). Uric acid transport, transporters, and their pharmacological targeting. Acta Physiol. *238*, e13980. https://doi.org/10.1111/apha.13980.
4. Pou Casellas, C., Jansen, K., Rookmaaker, M.B., Clevers, H., Verhaar, M.C., and Masereeuw, R. (2022). Regulation of solute carriers oct2 and OAT1/3 in the kidney: a phylogenetic, ontogenetic, and cell dynamic perspective. Physiol. Rev. *102*, 993–1024. https://doi.org/10.1152/physrev.00009.2021.
5. So, A., and Thorens, B. (2010). Uric acid transport and disease. J. Clin. Invest. *120*, 1791–1799. https://doi.org/10.1172/JCI42344.
6. Johnson, R.J., Nakagawa, T., Jalal, D., Sánchez-Lozada, L.G., Kang, D.H., and Ritz, E. (2013). Uric acid and chronic kidney disease: which is chasing which? Nephrol. Dial. Transplant. *28*, 2221–2228. https://doi.org/10.1093/ndt/gft029.
7. Fathallah-Shaykh, S.A., and Cramer, M.T. (2014). Uric acid and the kidney. Pediatr. Nephrol. *29*, 999–1008. https://doi.org/10.1007/s00467-013-2549-x.
8. Borghi, C., Agabiti-Rosei, E., Johnson, R.J., Kielstein, J.T., Lurbe, E., Mancia, G., Redon, J., Stack, A.G., and Tsioufis, K.P. (2020). Hyperuricaemia and gout in cardiovascular, metabolic and kidney disease. Eur. J. Intern. Med. *80*, 1–11. https://doi.org/10.1016/j.ejim.2020.07.006.
9. Bardin, T., and Richette, P. (2017). Impact of comorbidities on gout and hyperuricaemia: an update on prevalence and treatment options. BMC Med. *15*, 123. https://doi.org/10.1186/s12916-017-0890-9.
10. Gibson, T. (2012). Hyperuricemia, gout and the kidney. Curr. Opin. Rheumatol. *24*, 127–131. https://doi.org/10.1097/BOR.0b013e32834f049f.
11. Dhillon, S. (2019). Dapagliflozin: A Review in Type 2 Diabetes. Drugs *79*, 1135–1146. https://doi.org/10.1007/s40265-019-01148-3.
12. Chertow, G.M., Vart, P., Jongs, N., Toto, R.D., Gorriz, J.L., Hou, F.F., McMurray, J.J.V., Correa-Rotter, R., Rossing, P., Sjöström, C.D., et al. (2021). Effects of Dapagliflozin in Stage 4 Chronic Kidney Disease. J. Am. Soc. Nephrol. *32*, 2352–2361. https://doi.org/10.1681/ASN.2021020167.
13. Wheeler, D.C., Stefánsson, B.V., Jongs, N., Chertow, G.M., Greene, T., Hou, F.F., McMurray, J.J.V., Correa-Rotter, R., Rossing, P., Toto, R.D., et al. (2021). Effects of dapagliflozin on major adverse kidney and cardiovascular events in patients with diabetic and non-diabetic chronic kidney disease: a prespecified analysis from the DAPA-CKD trial. Lancet Diabetes Endocrinol. *9*, 22–31. https://doi.org/10.1016/S2213-8587(20)30369-7.
14. Lu, Y.H., Chang, Y.P., Li, T., Han, F., Li, C.J., Li, X.Y., Xue, M., Cheng, Y., Meng, Z.Y., Han, Z., et al. (2020). Empagliflozin Attenuates Hyperuricemia by Upregulation of ABCG2 via AMPK/AKT/CREB Signaling Pathway in Type 2 Diabetic Mice. Int. J. Biol. Sci. *16*, 529–542. https://doi.org/10.7150/ijbs.33007.
15. McDowell, K., Welsh, P., Docherty, K.F., Morrow, D.A., Jhund, P.S., de Boer, R.A., O'Meara, E., Inzucchi, S.E., Køber, L., Kosiborod, M.N., et al. (2022). Dapagliflozin reduces uric acid concentration, an independent predictor of adverse outcomes in DAPA-HF. Eur. J. Heart Fail. *24*, 1066–1076. https://doi.org/10.1002/ejhf.2433.
16. Butt, J.H., Docherty, K.F., Claggett, B.L., Desai, A.S., Petersson, M., Langkilde, A.M., de Boer, R.A., Hernandez, A.F., Inzucchi, S.E., Kosiborod, M.N., et al. (2023). Association of Dapagliflozin Use With Clinical Outcomes and the Introduction of Uric Acid-Lowering Therapy and Colchicine in Patients With Heart Failure With and Without Gout: A Patient-Level Pooled Meta-analysis of DAPA-HF and DELIVER. JAMA Cardiol. *8*, 386–393. https://doi.org/10.1001/jamacardio.2022.5608.
17. Hayashi, K., Mita, K., and Sawa, T. (2010). Electroencephalographic changes in the late cardiopulmonary bypass period are not reflected in the bispectral index. Clin. Neurophysiol. *121*, 1198–1204. https://doi.org/10.1016/j.clinph.2010.03.018.
18. Tin, A., Marten, J., Halperin Kuhns, V.L., Li, Y., Wuttke, M., Kirsten, H., Sieber, K.B., Qiu, C., Gorski, M., Yu, Z., et al. (2019). Target genes, variants, tissues and transcriptional pathways influencing human serum urate levels. Nat. Genet. *51*, 1459–1474. https://doi.org/10.1038/s41588-019-0504-x.
19. Pan, Z., Wang, K., Wang, X., Jia, Z., Yang, Y., Duan, Y., Huang, L., Wu, Z.X., Zhang, J.Y., and Ding, X. (2022). Cholesterol promotes EGFR-TKIs resistance in NSCLC by inducing EGFR/Src/Erk/SP1 signaling-mediated ERRalpha re-expression. Mol. Cancer *21*, 77. https://doi.org/10.1186/s12943-022-01547-3.
20. Kokabu, T., Mori, T., Matsushima, H., Yoriki, K., Kataoka, H., Tarumi, Y., and Kitawaki, J. (2019). Antitumor effect of XCT790, an ERRalpha inverse agonist, on ERalpha-negative endometrial cancer cells. Cell. Oncol. *42*, 223–235. https://doi.org/10.1007/s13402-019-00423-5.
21. Nigam, S.K. (2018). The SLC22 Transporter Family: A Paradigm for the Impact of Drug Transporters on Metabolic Pathways, Signaling, and Disease. Annu. Rev. Pharmacol. Toxicol. *58*, 663–687. https://doi.org/10.1146/annurev-pharmtox-010617-052713.
22. Euteneuer, A.M., Seeger-Nukpezah, T., Nolte, H., and Henjakovic, M. (2019). Estrogen receptor alpha (ERalpha) indirectly induces transcription of human renal organic anion transporter 1 (OAT1). Phys. Rep. *7*, e14229. https://doi.org/10.14814/phy2.14229.
23. Luo, J., Chen, S., Wang, L., Zhao, X., and Piao, C. (2022). Pharmacological effects of polydatin in the treatment of metabolic diseases: A review. Phytomedicine *102*, 154161. https://doi.org/10.1016/j.phymed.2022.154161.
24. Harlacher, E., Wollenhaupt, J., Baaten, C.C.F.M.J., and Noels, H. (2022). Impact of Uremic Toxins on Endothelial Dysfunction in Chronic Kidney Disease: A Systematic Review. Int. J. Mol. Sci. *23*, 531. https://doi.org/10.3390/ijms23010531.
25. Shi, Y., Tao, M., Chen, H., Ma, X., Wang, Y., Hu, Y., Zhou, X., Li, J., Cui, B., Qiu, A., et al. (2023). Ubiquitin-specific protease 11 promotes partial epithelial-to-mesenchymal transition by deubiquitinating the epidermal growth factor receptor during kidney fibrosis. Kidney Int. *103*, 544–564. https://doi.org/10.1016/j.kint.2022.11.027.
26. Beernink, J.M., Persson, F., Jongs, N., Laverman, G.D., Chertow, G.M., McMurray, J.J.V., Langkilde, A.M., Correa-Rotter, R., Rossing, P., Sjöström, C.D., et al. (2023). Efficacy of Dapagliflozin by Baseline Diabetes Medications: A Prespecified Analysis From the DAPA-CKD Study. Diabetes Care *46*, 602–607. https://doi.org/10.2337/dc22-1514.
27. Schechter, M., Jongs, N., Chertow, G.M., Mosenzon, O., McMurray, J.J.V., Correa-Rotter, R., Rossing, P., Langkilde, A.M., Sjöström, C.D., Toto, R.D., et al. (2023). Effects of Dapagliflozin on Hospitalizations in Patients With Chronic Kidney Disease : A Post Hoc Analysis of DAPA-CKD. Ann. Intern. Med. *176*, 59–66. https://doi.org/10.7326/M22-2115.

28. Tang, H.Y., Huang, J.E., Tsau, M.T., Chang, C.J., Tung, Y.C., Lin, G., and Cheng, M.L. (2023). Metabolomics Assessment of Volume Overload-Induced Heart Failure and Oxidative Stress in the Kidney. Metabolites *13*, 1165. https://doi.org/10.3390/metabo13111165.

29. Yu, W., Xiong, Y., Liu, M., Zeng, D., Zhao, H., Liu, J., and Lu, W. (2023). Structural analysis and attenuates hyperuricemic nephropathy of dextran from the Imperata cylindrica Beauv. var. major (Nees) C. E. Hubb. Carbohydr. Polym. *317*, 121064. https://doi.org/10.1016/j.carbpol.2023.121064.

30. Cui, J., Hong, P., Li, Z., Lin, J., Wu, X., Nie, K., Zhang, X., and Wan, J. (2023). Chloroquine inhibits NLRP3 inflammasomes activation and alleviates renal fibrosis in mouse model of hyperuricemic nephropathy with aggravation by a high-fat-diet. Int. Immunopharmacol. *120*, 110353. https://doi.org/10.1016/j.intimp.2023.110353.

31. Lin, N.Y.C., Homan, K.A., Robinson, S.S., Kolesky, D.B., Duarte, N., Moisan, A., and Lewis, J.A. (2019). Renal reabsorption in 3D vascularized proximal tubule models. Proc. Natl. Acad. Sci. USA *116*, 5399–5404. https://doi.org/10.1073/pnas.1815208116.

32. Gewin, L.S. (2018). Renal fibrosis: Primacy of the proximal tubule. Matrix Biol. *68–69*, 248–262. https://doi.org/10.1016/j.matbio.2018.02.006.

33. Wang, Z., Cui, T., Ci, X., Zhao, F., Sun, Y., Li, Y., Liu, R., Wu, W., Yi, X., and Liu, C. (2019). The effect of polymorphism of uric acid transporters on uric acid transport. J. Nephrol. *32*, 177–187. https://doi.org/10.1007/s40620-018-0546-7.

34. Ermakov, V.S., Granados, J.C., and Nigam, S.K. (2023). Remote effects of kidney drug transporter OAT1 on gut microbiome composition and urate homeostasis. JCI Insight *8*, e172341. https://doi.org/10.1172/jci.insight.172341.

35. Schneider, R., Meusel, M., Betz, B., Held, C., Möller-Ehrlich, K., Büttner-Herold, M., Wanner, C., Gekle, M., and Sauvant, C. (2015). Oat1/3 restoration protects against renal damage after ischemic AKI. Am. J. Physiol. Ren. Physiol. *308*, F198–F208. https://doi.org/10.1152/ajprenal.00160.2014.

36. Chang, L. (2023). OAT1 structures reveal insights into drug transport in the kidney. Nat. Struct. Mol. Biol. *30*, 1615–1617. https://doi.org/10.1038/s41594-023-01144-y.

37. Granados, J.C., Nigam, A.K., Bush, K.T., Jamshidi, N., and Nigam, S.K. (2021). A key role for the transporter OAT1 in systemic lipid metabolism. J. Biol. Chem. *296*, 100603. https://doi.org/10.1016/j.jbc.2021.100603.

38. Vavra, J., Mancikova, A., Pavelcova, K., Hasikova, L., Bohata, J., and Stiburkova, B. (2022). Functional Characterization of Rare Variants in OAT1/SLC22A6 and OAT3/SLC22A8 Urate Transporters Identified in a Gout and Hyperuricemia Cohort. Cells *11*, 1063. https://doi.org/10.3390/cells11071063.

39. Khan, D., Ara, T., Ravi, V., Rajagopal, R., Tandon, H., Parvathy, J., Gonzalez, E.A., Asirvatham-Jeyaraj, N., Krishna, S., Mishra, S., et al. (2021). SIRT6 transcriptionally regulates fatty acid transport by suppressing PPARgamma. Cell Rep. *35*, 109190. https://doi.org/10.1016/j.celrep.2021.109190.

40. Song, W., Li, D., Tao, L., Luo, Q., and Chen, L. (2020). Solute carrier transporters: the metabolic gatekeepers of immune cells. Acta Pharm. Sin. B *10*, 61–78. https://doi.org/10.1016/j.apsb.2019.12.006.

41. He, F., Ru, X., and Wen, T. (2020). NRF2, a Transcription Factor for Stress Response and Beyond. Int. J. Mol. Sci. *21*, 4777. https://doi.org/10.3390/ijms21134777.

42. Zhou, S., and Shu, Y. (2022). Transcriptional Regulation of Solute Carrier (SLC) Drug Transporters. Drug Metab. Dispos. *50*, 1238–1250. https://doi.org/10.1124/dmd.121.000704.

43. Eraly, S.A., Hamilton, B.A., and Nigam, S.K. (2003). Organic anion and cation transporters occur in pairs of similar and similarly expressed genes. Biochem. Biophys. Res. Commun. *300*, 333–342. https://doi.org/10.1016/s0006-291x(02)02853-x.

44. Crevet, L., and Vanacker, J.M. (2020). Regulation of the expression of the estrogen related receptors (ERRs). Cell. Mol. Life Sci. *77*, 4573–4579. https://doi.org/10.1007/s00018-020-03549-0.

45. Dhillon, P., Park, J., Hurtado Del Pozo, C., Li, L., Doke, T., Huang, S., Zhao, J., Kang, H.M., Shrestra, R., Balzer, M.S., et al. (2021). The Nuclear Receptor ESRRA Protects from Kidney Disease by Coupling Metabolism and Differentiation. Cell Metab. *33*, 379–394.e8. https://doi.org/10.1016/j.cmet.2020.11.011.

46. Wang, X.X., Myakala, K., Libby, A.E., Krawczyk, E., Panov, J., Jones, B.A., Bhasin, K., Shults, N., Qi, Y., Krausz, K.W., et al. (2023). Estrogen-Related Receptor Agonism Reverses Mitochondrial Dysfunction and Inflammation in the Aging Kidney. Am. J. Pathol. *193*, 1969–1987. https://doi.org/10.1016/j.ajpath.2023.07.008.

47. Tsushida, K., Tanabe, K., Masuda, K., Tanimura, S., Miyake, H., Arata, Y., Sugiyama, H., and Wada, J. (2018). Estrogen-related receptor alpha is essential for maintaining mitochondrial integrity in cisplatin-induced acute kidney injury. Biochem. Biophys. Res. Commun. *498*, 918–924. https://doi.org/10.1016/j.bbrc.2018.03.080.

48. Wang, D., Wang, Y., Liu, F.Q., Yuan, Z.Y., and Mu, J.J. (2016). High Salt Diet Affects Renal Sodium Excretion and ERRalpha Expression. Int. J. Mol. Sci. *17*, 480. https://doi.org/10.3390/ijms17040480.

49. Narang, R.K., Vincent, Z., Phipps-Green, A., Stamp, L.K., Merriman, T.R., and Dalbeth, N. (2019). Population-specific factors associated with fractional excretion of uric acid. Arthritis Res. Ther. *21*, 234. https://doi.org/10.1186/s13075-019-2016-6.

50. Hirai, T., Kawagoe, Y., Kei, M., Ogawa, R., and Itoh, T. (2020). Clinical Predictors of the Hypoglycemic Effect of Sodium-Glucose Co-transporter-2 Inhibitors in Hyperuricemic Patients: A Retrospective Descriptive Observational Study. Biol. Pharm. Bull. *43*, 782–787. https://doi.org/10.1248/bpb.b19-00785.

51. Ren, Q., Wang, B., Guo, F., Huang, R., Tan, Z., Ma, L., and Fu, P. (2021). Natural Flavonoid Pectolinarigenin Alleviated Hyperuricemic Nephropathy via Suppressing TGFbeta/SMAD3 and JAK2/STAT3 Signaling Pathways. Front. Pharmacol. *12*, 792139. https://doi.org/10.3389/fphar.2021.792139.

52. Wei, R., Cui, X., Feng, J., Gu, L., Lang, S., Wei, T., Yang, J., Liu, J., Le, Y., Wang, H., et al. (2020). Dapagliflozin promotes beta cell regeneration by inducing pancreatic endocrine cell phenotype conversion in type 2 diabetic mice. Metabolism *111*, 154324. https://doi.org/10.1016/j.metabol.2020.154324.

53. Terryn, S., Jouret, F., Vandenabeele, F., Smolders, I., Moreels, M., Devuyst, O., Steels, P., and Van Kerkhove, E. (2007). A primary culture of mouse proximal tubular cells, established on collagen-coated membranes. Am. J. Physiol. Ren. Physiol. *293*, F476–F485. https://doi.org/10.1152/ajprenal.00363.2006.

54. Sancho-Martinez, S.M., Herrero, M., Fontecha-Barriuso, M., Mercado-Hernandez, J., and Lopez-Hernandez, F.J. (2022). The Urinary Level of Injury Biomarkers Is Not Univocally Reflective of the Extent of Toxic Renal Tubular Injury in Rats. Int. J. Mol. Sci. *23*, 3494. https://doi.org/10.3390/ijms23073494.

55. Cao, Y., Chen, X., Zhu, Z., Luo, Z., Hao, Y., Yang, X., Feng, J., Zhang, Z., Hu, J., Jian, Y., et al. (2024). STING contributes to lipopolysaccharide-induced tubular cell inflammation and pyroptosis by activating endoplasmic reticulum stress in acute kidney injury. Cell Death Dis. *15*, 217. https://doi.org/10.1038/s41419-024-06600-1.

56. Hu, H., Li, W., Hao, Y., Peng, Z., Zou, Z., and Liang, W. (2024). Baicalin ameliorates renal fibrosis by upregulating CPT1alpha-mediated fatty acid oxidation in diabetic kidney disease. Phytomedicine *122*, 155162. https://doi.org/10.1016/j.phymed.2023.155162.

57. Bonnet, H., Coche-Guérente, L., Defrancq, E., Spinelli, N., Van der Heyden, A., and Dejeu, J. (2021). Negative SPR Signals during Low Molecular Weight Analyte Recognition. Anal. Chem. *93*, 4134–4140. https://doi.org/10.1021/acs.analchem.1c00071.

58. Entzian, C., and Schubert, T. (2016). Studying small molecule-aptamer interactions using MicroScale Thermophoresis (MST). Methods *97*, 27–34. https://doi.org/10.1016/j.ymeth.2015.08.023.

59. Lomenick, B., Hao, R., Jonai, N., Chin, R.M., Aghajan, M., Warburton, S., Wang, J., Wu, R.P., Gomez, F., Loo, J.A., et al. (2009). Target identification using drug affinity responsive target stability (DARTS). Proc. Natl. Acad. Sci. USA *106*, 21984–21989. https://doi.org/10.1073/pnas.0910040106.

60. Martinez Molina, D., Jafari, R., Ignatushchenko, M., Seki, T., Larsson, E.A., Dan, C., Sreekumar, L., Cao, Y., and Nordlund, P. (2013). Monitoring drug target engagement in cells and tissues using the cellular thermal shift assay. Science *341*, 84–87. https://doi.org/10.1126/science.1233606.

STAR★METHODS

KEY RESOURCES TABLE

REAGENT or RESOURCE	SOURCE	IDENTIFIER
Antibodies		
ERRα	Genetex	Cat# GTX108166; RRID: AB_1950230
OAT1	Proteintech	Cat# 26574-1-AP; RRID: AB_2880557
FN1	Abcam	Cat# ab2413; RRID: AB_2262874
αSMA	Abcam	Cat# ab7817; RRID: AB_262054
TOM20	Abcam	Cat# ab186735; RRID: AB_2889972
SGLT2	Proteintech	Cat# 24654-1-AP; RRID: AB_2750601
β-actin	Abcam	Cat# ab8226; RRID: AB_306371
Bacterial and virus strains		
AAV-ERRα	Hanbio	N/A
AAV-Control	Hanbio	N/A
Biological samples		
Kidney samples from control patients	Renmin Hospital of Wuhan University	N/A
Kidney samples from HN patients	Renmin Hospital of Wuhan University	N/A
Kidney samples from HN + Dapa patients	Renmin Hospital of Wuhan University	N/A
Chemicals, peptides, and recombinant proteins		
Adenine	MCE	HY-B0152
Potassium oxonate	MCE	HY-17511
Dapagliflozin	MCE	HY-10450
Allopurinol	MCE	HY-B0219
Collagenase II	Roche	10103586001
Proteinase E	Sigma-Aldrich	D4527
Deoxyribonuclease I	Sigma-Aldrich	P6911
Uric acid	MCE	HY-B2130
TGF-β	MCE	HY-P7118
XCT-790	MCE	HY-10426
TRIzol	Invitrogen	15596018CN
SYBR Green PCR Master Mix	Vazyme	N/A
M-PER lysis buffer	Thermo	FNN0011
Critical commercial assays		
Cell counting kit-8	Beyotime	C0037
MitoTracker dye	Thermo	A66443
LTL dye	Lifespan	N/A
DAPI dye	Antgene	ANT063
Hoechst dye	Beyotime	P0133
DCFH-DA probe	Beyotime	S0033S
ATP Assay Kit	Beyotime	S0027
Mitochondrial Stress Test Kit	Agilent	103010–100
BCA assay kit	Beyotime	P0009
cDNA synthesis kit	Servicebio	G3333-50
Dual-luciferase reporter gene assay kit	Yeasen	11405ES60
Mouse urinary albumin-ELISA kit	Abcam	Ab207620
Deposited data		
Raw data files for ChIP-seq	This paper	SRA: PRJNA1137848
Raw data files for RNA-seq	This paper	SRA: PRJNA1137843

(*Continued on next page*)

Continued

REAGENT or RESOURCE	SOURCE	IDENTIFIER
Experimental models: Cell lines		
Human proximal tubule cell line (HK-2)	Procell	No. CP-H193
SGLT2-KO HK2 cell	Cyagen	N/A
ERRα-KO HK2 cell	Cyagen	N/A
Experimental models: Organisms/strains		
Mouse: C57BL/6N	Cyagen	C001072
Mouse: db/m	Cyagen	C001274
Mouse: db/db	Cyagen	C001291
Mouse: ERRα^{ptKI}	This paper	N/A
Mouse: ERRα^{Control}	This paper	N/A
Mouse: ERRα$^{fl/fl}$	Cyagen	S-CKO-09545
Mouse: Ggt1-Cre	Cyagen	C001028
Oligonucleotides		
si-ERRα	Sangon	N/A
si-Control	Sangon	N/A
Recombinant DNA		
Plasmid: pcDNA3.1-OAT1	Sangon	N/A
Plasmid: pcDNA3.1-Control	Sangon	N/A
Plasmid: pGL3-OAT1-WT	Genecreate	N/A
Plasmid: pGL3-OAT1-MUT	Genecreate	N/A
Plasmid: pcDNA3.1-ERRα	Genecreate	N/A
Software and algorithms		
ImageJ	National Institutes of Health	https://imagej.nih.gov/ij/
Bioinformatics	Shanghai NewCore Biotechnology Co., Ltd.	https://bioinformatics.com.cn
Bowtie version 1.1.2	Bowtie GitHub	https://bowtie-bio.sourceforge.net/
Genomic Ranges R package	GenomicRanges	https://bioconductor.org/
MACS v2.10	2008: Model-based Analysis of ChIP-Seq (MACS)	https://pypi.org/project/MACS2/
String	Database: String	https://string-db.org/
KPMP	Kidney Precision Medicine Project	https://www.kpmp.org
JASPAR	Database: JASPAR	https://jaspar.genereg.net/
NCBI	National Library of Medicine	https://ncbi.nlm.nih.gov
AutoDock Vina (version 1.1.2)	Center for Computational Structural Biology	https://vina.scripps.edu
PubChem	Database: PubChem	https://pubchem.ncbi.nlm.nih.gov
RCSB	Protein Data Bank: RCSB	https://rcsb.org
PyMOL (version 4.3.0)	Schr€odinger	https://pymol.org/
HDOCK	Lab of Biophysics and Molecular Modeling	https://hdock.phys.hust.edu.cn/
3dRNA web server	3dRNA Web Server	https://biophy.hust.edu.cn/new/3dRNA

RESOURCE AVAILABILITY

Lead contact

Further information and requests for resources should be directed to and will be fulfilled by the lead contact, Yun Cao (yuncao1223@hainmc.edu.cn).

Materials availability

This study did not generate unique reagents.

Data and code availability

All data associated with this study are present in the paper or the supplementary materials. RNA-seq data generated for this study are deposited at the Sequence Read Archive (SRA) in the NCBI database under the accession number PRJNA1137843. ChIP-seq data

generated for this study are deposited at the SRA in the NCBI database under the accession number PRJNA1137848. This paper does not report original code. Any additional information required to reanalyze the data reported in this paper is available from the lead contact upon request.

EXPERIMENTAL MODEL AND STUDY PARTICIPANT DETAILS

Human kidney biopsy specimens and clinical index collection

Control kidney samples were derived from non-diseased regions adjacent to cancerous tissues. HN kidney biopsy samples were harvested from patients pathologically diagnosed with HN. The patients included in the study had proteinuria (24-h urinary albumin excretion >150 mg for 3 months) and received either ARB or ARB plus dapagliflozin treatment. Therefore, they were divided into two groups: 1. HN: received basal ARB treatment (Irbesartan, 150 mg/day for a least 24 months), 2. HN + Dapa: received basal ARB treatment and dapagliflozin treatment (10 mg/day for a least 24 months). A comprehensive clinical index was compiled for all patients. Informed consent was obtained from all patients prior to inclusion in the study. Detailed clinical characteristics of the patients are summarized in Tables S1 and S2. The study received approval from the ethics committee of Renmin Hospital of Wuhan University to access the digital records of participants who provided informed consent to share their records with local institutions (WDRY2021-KS251).

Mouse studies

The mice were housed under specific pathogen-free conditions, with a controlled environment of 40–70% humidity and a temperature range of 20°C–25°C, following a 12-h light/12-h dark cycle. They were provided with free access to food and water. At the conclusion of the dosing cycle, humane euthanasia of all mice was conducted via intraperitoneal injection of pentobarbital sodium (200 mg/kg). Kidney samples were harvested for subsequent testing. The entire experimental procedure was conducted in a blinded fashion. All animal experiments adhered to the Guidelines for the Care and Use of Laboratory Animals (NIH publication, revised 2011) and obtained approval from the Ethical Committee for the Experimental Use of Animals at Renmin Hospital, Wuhan University, China (WDRM-20221941).

HN mice model construction and treatment

Male C57BL/6N mice (age: 6–8 weeks, weight: 20–25 g) were procured from Cyagen Biosciences Co., Ltd (China). To establish the HN mouse model, adenine (0.16 g/kg; MCE, USA) and potassium oxonate (2.4 g/kg; MCE, USA) mixture (dissolved in a 0.5% CMC-Na solution) were orally administered every other day for four weeks.[51] The control mice were given an equivalent volume of 0.5% CMC-Na solution via oral gavage, while HN mice were orally administered daily with dapagliflozin (MCE, USA) of 1.0 mg/kg or allopurinol (MCE, China) of 5.0 mg/kg for four weeks after the HN model was established.[52]

ERRα^{ptKI} mice generation and treatment

Tubule-specific ERRα (erythroblastosis virus E26 oncogene homolog 1) overexpression (ERRα^{ptKI}) mice were generated through the crossbreeding of ERRα$^{fl/fl}$ mice (C57BL/6N; Cyagen, China) and Ggt1-Cre mice (C57BL/6N; Cyagen, China). Additionally, littermates with homozygous floxed mice without Cre expression were categorized as ERRα^{Control}. Male ERRα^{Control} and ERRα^{ptKI} mice (aged 6–8 weeks and weighing 20–25 g) were randomly assigned for HN modeling. Subsequently, they were divided into 4 groups: ERRα^{Control}, ERRα^{ptKI}, ERRα^{Control}+HN and ERRα^{ptKI}+HN.

Obesity, type 2 DKD, UUO mice model construction and treatment

Male C57BL/6N mice (age: 6–8 weeks, weight: 20–25 g) were purchased from Cyagen Biosciences Co., Ltd. (China) and fed an HFD (60 kcal% from fat, Research Diets, USA) for eight weeks to establish an obesity mouse model. Male db/db mice and matched db/m mice (age: 6–8 weeks, weight: 20–25 g) were purchased from Cyagen Biosciences Co., Ltd (China) and fed until they reached 16 weeks of age to establish a type 2 DKD mice model. Male C57BL/6N mice (age: 6–8 weeks, weight: 20–25 g) were purchased from Cyagen Biosciences Co., Ltd (China) and anesthetized with 30% isoflurane. A mid-abdominal incision was made to expose the left ureter. The left ureter was ligated with a silk suture to induce the ureteral obstruction (UUO) model. The UUO mice were maintained in a breeding facility for 14 days following the closure of the incision. Following the successful construction of the obesity, type 2 DKD, UUO mice model, a 4-week treatment with dapagliflozin (1.0 mg/kg) was initiated.

HK-2 cell culture and treatment

The human proximal tubule cell line (HK-2), acquired from Procell (China), was cultured in DMEM/F12 medium (Hyclone, USA) supplemented with 10% fetal bovine serum (Corning, USA) and 1% penicillin-streptomycin (Biosharp, China) at 37°C in a 5% CO_2 incubator. UA (MCE, China) stimulation in HK-2 cells: 400 μM, 48 h. dapagliflozin treatment in in HK-2 cells: 10 μM, 48 h. HG treatment in HK-2 cells: 30 mM, 48 h. TGF-β (MCE, China) treatment in HK-2 cells: 10 ng/mL, 48 h. XCT-790 (MCE, China) treatment in HK-2 cells: 10 μM, 24 h.

SGLT2-or ERRα-KO HK-2 cell line construction and treatment

In brief, SGLT2-and ERRα-KO HK-2 cell lines were constructed by Cyagen Biosciences Co., Ltd. (China) using CRISPR/Cas9 technology. This involved gene information analysis, sgRNA design and synthesis, cell transfection, monoclonal screening and sequencing identification. The UA stimulation was applied to SGLT2-or ERRα-KO HK-2 cells at a concentration of 400 μM for a period of 48 h. Dapagliflozin was administered to SGLT2-or ERRα-KO HK-2 cells at a concentration of 10 μM for a period of 48 h

METHOD DETAILS

Isolation of renal tubules

The isolation of renal tubules was performed using a modified sieving method as described previously.[53] Before removing the kidney, it was perfused with a sterile Hanks balanced salt solution (HBSS). Renal cortex was separated from medulla and cut into 1mm3 pieces with a scalpel and then digested in a solution containing collagenase II (Roche, Swit), proteinase E (Sigma-Aldrich, USA), and deoxyribonuclease I (Sigma-Aldrich, USA) at 37°C for 30 min. After digestion, the samples were sequentially pressed through 100-, 70-, 40-μm cell strainer (BD, USA; Greiner bio-one, German) to get renal tubules. Finally, the cell suspension was centrifuged at 1500 rpm for 5 min at 4°C, and the pellets were re-suspended in a 5 mL culture medium.

Renal functional parameters measurement

Prior to sacrifice, blood samples were harvested from the orbital sinus of the mice. The collected samples were then analyzed utilizing an automated biochemical analyzer (Beckman, USA) to assess serum UA, Cr, and BUN levels. In addition, the mice were individually housed in metabolic cages for 24 h to collect urine samples. These urine samples were centrifuged at 1000 g and 4°C for 10 min to isolate the supernatant. An ELISA kit (Abcam, USA) was utilized to quantify urinary albumin levels. Finally, UACR was calculated based on urinary albumin level and Scr.

Cell viability assay

The effect of dapagliflozin on cell viability under UA exposure was evaluated utilizing the cell counting kit-8 (CCK-8; Beyotime, China). HK-2 cells were seeded in 96-well plates and treated with varying concentrations of UA (0 or 400 μM) and dapagliflozin (0, 5, 10, or 20 μM) for 48 h. Following this, 10 μL of CCK-8 solution was added to each well and incubated for 1 h at 37°C in a 5% CO_2 incubator. The absorbance was measured at 450 nm utilizing a microplate reader (PerkinElmer, USA).

Cell transfection

The ERRα small interfering RNA (si-ERRα) and OAT1 full-length expression plasmid (OE-OAT1), obtained from Sangon (China), were transfected into TECS or HK-2 cells utilizing HiPerFect Transfection Reagent (Qiagen, Germany) and X-tremeGENE HP DNA Transfection Reagent (Roche, Swit). The adeno-associated virus carrying the ERRα gene (AAV-ERRα) or control (AAV-Control) was generated by Hanbio (China) and transfected into TECS or HK-2 cells. 48 h UA stimulation was added after 24 h of transfection. TECS or HK-2 cells were collected for subsequent experiments.

Histological and IHC analysis

Fixed renal tissues obtained from patients or mice were processed by dehydration and paraffin embedding. Subsequently, the kidney sections were deparaffinized, hydrated, and antigen-repaired. For histological analysis, kidney sections were subjected to staining with Hematoxylin-Eosin (HE), Masson, and Sirius red reagents to visualize renal histopathological changes. The average values of tubular injury score[54] and the area of positive staining for Masson/Sirius red were evaluated in each group using 30 randomly selected non-overlapping fields (Five visual fields for each section analyzed).

Regarding IHC, kidney sections were blocked with 5% bovine serum albumin (BSA) for 1 h at room temperature, followed by incubation overnight at 4°C with primary antibodies such as ERRα (Genetex, USA) and OAT1 (Proteintech, China). Then, kidney sections were incubated with HRP-conjugated secondary antibodies for 1 h at room temperature. Immunoreactivity was detected using diaminobenzidine as the substrate. All microscopic images were captured utilizing an upright microscope (Olympus, Japan).

If assay

The kidney sections from patients or mice underwent the same pretreatment as described for IHC. In addition, cell-climbing films of TECs or HK-2 cells were fixed and blocked with 5% BSA at room temperature for 1 h. Following this, the kidney sections and cell-climbing films were incubated overnight at 4°C with primary antibodies, including Fibronectin1 (FN1; Abcam, UK), α-smooth muscle actin (αSMA; Abcam, UK), ERRα, and OAT1. Subsequently, kidney sections and cell-climbing films were incubated with HRP-conjugated secondary antibodies for 1 h. Mitochondria were marked using TOM20 antibody (abcam, UK) or MitoTracker dye (Thermo, USA). Proximal renal tubules were marked using LTL dye (Lifespan, China). Nuclei were stained using an antifade mounting medium with DAPI (Antgene, China) or Hoechst (Beyotime, China). All microscopic images were captured employing a confocal microscope

(Olympus, Japan). The average fluorescence intensity, mitochondrial morphology values were assessed by analyzing 15 randomly selected, non-overlapping fields in each group (Five visual fields for each section analyzed).

ROS and ATP analysis

According to the manufacturer's instructions, ROS level was measured by a DCFH-DA fluorescent probe (Beyotime, China), visualized by an inverted microscopy (Olympus, Japan). ATP level was measured by an ATP Assay Kit (Beyotime, China), and quantified by a microplate reader (Bio-rad, USA).[55]

OCR detection

Mitochondrial oxygen consumption was evaluated utilizing a Mitochondrial Stress Test Kit (Agilent, USA). To measure the OCR, a Seahorse Bioscience XFe96 Extracellular Flux Analyzer (Seahorse Bioscience, USA) was employed, following a previously established procedure.[56]

TEM

Renal cortex samples from patients and mice, as well as TECs and HK-2 cells, were collected and processed by fixation, dehydration, and embedding in epoxy resin. The mitochondrial morphology and structure in renal TECs and HK-2 cells were examined using a TEM (Hitachi, Japan). *In vivo*, mitochondrial aspect ratio, circularity, and roundness were calculated for 64 (control patient) or 130 (HN patient, mice) mitochondria. *In vitro*, the mitochondrial inner mitochondrial membrane (IMM)/outer mitochondrial membrane (OMM) ratio, total cristae length/mitochondrial area, and cristae junction/mitochondrial area were calculated by 130 mitochondria.

WB analysis

Initially, the renal cortices from mice or TECs or HK-2 cells were subjected to protein extraction, and their concentrations were determined utilizing the BCA assay kit (Beyotime, Shanghai). Subsequently, an equal amount of protein was separated by 8–12% SDS-PAGE gels and transferred onto PVDF membranes (Millipore, USA). The membranes were then blocked with 5% skim milk at room temperature for 1 h, followed by overnight incubation at 4°C with primary antibodies, including FN1, αSMA, ERRα, SGLT2 (Proteintech, China), OAT1, and β-actin (Abcam, UK). Afterward, the membranes were incubated with HRP-conjugated secondary antibodies for 1 h at room temperature. Following this, the membranes were treated with ECL buffer (Abbkine, China), and the bands were visualized using a chemiluminescence imaging system (Monad, China). ImageJ software was employed for quantifying the grayscale of the bands.

RNA extraction and qRT-PCR analysis

In accordance with the manufacturer's instructions, TRIzol reagent (Invitrogen, USA) was employed to isolate total RNA. A total of 1 μg of RNA was reverse transcribed using a cDNA synthesis kit (Servicebio, China). Quantitative reverse transcription polymerase chain reaction (qRT-PCR) analysis was then performed to detect mRNA expression levels using SYBR Green PCR Master Mix (Vazyme, Nanjing, China) in a real-time PCR system (Bio-Rad, USA).[55] The primers utilized are detailed in Table S3.

Bulk RNA-seq analysis

The HK-2 cells from both the control and si-ERRα groups were collected and immersed in TRIZOL buffer, then rapidly frozen and stored in liquid nitrogen. RNA-seq analysis was performed by Novogene Co., Ltd. Differentially expressed genes (DEGs) were implemented utilizing DESeq2 with a significance threshold set at adjusted $p < 0.05$. The chord diagram was generated on an online platform for data analysis and visualization (bioinformatics.com.cn).

ChIP-seq analysis

HK-2 cells were collected and treated with 1% paraformaldehyde for 15 min to facilitate crosslinking. Subsequently, 125 mM glycine was added to halt the crosslinking process. ChIP-seq analysis was performed by igenebook Co., Ltd. The ChIP-seq reads were aligned to the genome of HK-2 cells using Bowtie version 1.1.2. To generate ChIP-seq coverage plots, the locations of the mapped ChIP-seq reads were extended to 150 bp, representing the sequenced fragments. Big-Wig files were generated using the genomic Ranges R package. Peaks were called using MACS v2.10 with a significance cut-off value of ≤ 0.01. The score assigned to each peak represents the normalized coverage of DNA fragments at a specific genomic coordinate. Narrow Peak files were generated using MACS v2 with default settings.

Dual-luciferase reporter assay

Dual-luciferase reporter assay was conducted by Genecreate Biosciences Co., Ltd. (China). In short, a target sequence of approximately 200 base pairs (WT or MUT) in the promoter region of the OAT1 gene was inserted into the pGL3-basic plasmid. The coding sequence of the ERRα protein gene was inserted into the pcDNA3.1 plasmid. 293T cells were transfected randomly with the plasmids and divided into four groups: pcDNA3.1-NC+OAT1-WT, pcDNA3.1-NC+OAT1-MUT, pcDNA3.1-ERRα+OAT1-WT, and pcDNA3.1-

ERRα+OAT1-MUT. After transfection, the 293T cells were subjected to a dual-luciferase reporter gene assay kit (Yeasen, China). Luciferase activity was measured utilizing a luminometer (Promega, USA).

GEO dataset and single-nucleus RNA-seq dataset analyses

The GSE190205 dataset were obtained from the Gene Expression Omnibus (GEO) database (ncbi.nlm.nih.gov/geo/) and analyzed on an online platform for data analysis and visualization: bioinformatics.com.cn. DEGs were identified using DESeq2 (adjusted $p < 0.05$). Heatmaps were generated to display altered gene expression. A Volcano plot was employed to identify up-regulated or down-regulated genes, which exhibited a p-value < 0.05 and |fold change| >1.0, and these genes were highlighted in red or blue. Gene ontology (GO) enrichment analysis was conducted to explore critical pathways involved in HN progression. The String website: string-db.org/ was utilized to map the molecular function network.

The single-nucleus RNA-seq data was analyzed using the Kidney Precision Medicine Project: interstitial.org. The application of the Uniform Manifold Approximation and Projection (UMAP) technique allowed for the visualization of distinct clusters of renal cells, enabling the identification of ERRα-positive cell localization in both healthy individuals and patients with CKD.

Motif prediction

In this study, the promoter sequence of the OAT1 gene was retrieved from the NCBI website: ncbi.nlm.nih.gov. The JASPAR database, jaspar.genereg.net/, was then utilized to search for the ERRα motif (homo sapiens) and retrieve its TF flexible model logo. Next, the obtained promoter sequence of the OAT1 gene was uploaded to the JASPAR database to identify the binding site between the ERRα protein and the OAT1 gene.

Molecular docking method

XCT-790/Dapagliflozin-ERRα protein docking was completed utilizing AutoDock Vina (version 1.1.2). The structure of XCT-790 and Dapagliflozin (as the ligand) was retrieved from PubChem, while the ERRα protein (as the receptor) was obtained from the RCSB database. For the analysis and visualization of the resulting forces in both 3D and 2D perspectives, PyMOL (version 4.3.0) software (pymol.org/) and Discovery Studio software were employed.

The ERRα protein-OAT1 gene docking was implemented utilizing the HDOCK website: hdock.phys.hust.edu.cn/. The ERRα protein was obtained from the RCSB database, while the tertiary structure of the OAT1 gene was modeled using the 3dRNA web server. The analysis and visualization of the interaction between the amino acid residues and bases in the ERRα protein-OAT1 gene complex were completed employing PyMOL software.

SPR analysis

SPR analysis was conducted by Yangene Biosciences Co., Ltd. (China). In accordance with the manufacturer's instructions, three steps were undertaken to calculate the affinity of dapagliflozin to the ERRα protein (ligand). These were: chip preparation, ligand immobilisation and running the analyte using the multi-cycle method.[57]

MST analysis

The MST analysis was conducted by Yangene Biosciences Co., Ltd. (China). In accordance with the manufacturer's instructions, three steps were undertaken to calculate the affinity of dapagliflozin (ligand) to ERRα protein (ligand). These comprised protein labeling, a binding assay and analysis.[58]

DARTS

DARTS assays were completed following the instructions provided by the manufacturer.[59] In brief, TECS or HK-2 cells were incubated with M-PER lysis buffer (Thermo, USA) at 4°C for 10 min. The cell lysates were collected and centrifuged, followed by protein concentration determination. Subsequently, the cell lysates were incubated with either DMSO or dapagliflozin (10 μM) at room temperature for 2 h. Each sample was then exposed to streptavidin (Roche, Swit) at concentrations of 0, 25, 50, and 125 ng, and subjected to proteolytic hydrolysis at room temperature for 10 min. The proteolysis was terminated by adding a pre-cooled protease inhibitor mixture, followed by further termination through boiling at 95°C for 10 min. Finally, each sample was loaded onto an SDS-PAGE gel for WB analysis.

CETSA

CETSA was performed in accordance with the manufacturer's guidelines.[60] The total protein from TECS or HK-2 cells was extracted, and then divided into two equal portions. Each portion was separately incubated, one with DMSO and the other with dapagliflozin (10 μM), at room temperature for 2 h. Subsequently, each set of lysates was divided into seven equal fractions and heated at temperatures of 37, 42, 47, 52, 57, 62, 67°C and 72°C for 3 min. Finally, all the samples were loaded onto an SDS-PAGE gel for subsequent WB analysis.

QUANTIFICATION AND STATISTICAL ANALYSIS

All experiments were conducted a minimum of three times. Data analysis was performed using GraphPad Prism 8. The data were presented as means ± standard error of mean and were derived from the indicated number of independent experiments. Statistical comparisons between groups were carried out using a one-way analysis of variance followed by a Tukey's post-test. Kaplan-Meier survival analysis and log rank tests were employed to assess the incidence of a 2-fold increase in Scr onset with regular two-month follow-up visits for 24 months in subjects belonging to different groups. Pearson correlation analysis was used to evaluate the correlations between numerical variables. A p-value of less than 0.05 was deemed statistically significant.